DOI: 10.1002/chem.200601089

Chemical and Constitutional Influences in the Self-Assembly of Functional Supramolecular Hydrogen-Bonded Nanoscopic Fibres

Josep Puigmartí-Luis,[a] Andrea Minoia,[b] Ángel Pérez del Pino,[a] Gregori Ujaque,[c] Concepció Rovira,[a] Agustí Lledós,[c] Roberto Lazzaroni,[b] and David B. Amabilino*[a]

Abstract: A new series of secondary amides bearing long alkyl chains with π-electron-donor cores has been synthesized and characterised, and their self-assembly upon casting at surfaces has been studied. The different supramolecular assemblies of the materials have been visualized by using atomic force microscopy (AFM) and transmission electron microscopy (TEM). It is possible to obtain well-defined fibres of these aromatic core molecules as a result of the hydrogen bonds between the amide groups. Indeed, by altering the alkyl-chain lengths, constitutions, concentrations and solvent, it is possible to form different rodlike aggregates on graphite. Aggregate sizes with a lower limit of 6–8 nm width have been reached for different amide derivatives, while others show larger aggregates with rodlike morphologies which are several micrometers in length. For one compound that forms nanofibres, doping was performed by using a chemical oxidant, and the resulting layer on graphite was shown to exhibit metallic-like spectroscopy curves when probed with current-sensing AFM. This technique also revealed current maps of the surface of the molecular material. Fibre formation not only takes place on the graphite surface: nanometre scale rods have been imaged by using TEM on a grid after evaporation of solutions of the compounds in chloroform. Molecular modelling proves the importance of the hydrogen bonds in the generation of the fibres, and indicates that the constitution of the molecules is vital for the formation of the desired columnar stacks, results that are consistent with the images obtained by microscopic techniques. The results show the power of noncovalent bonds in self-assembly processes that can lead to electrically conducting nanoscale supramolecular wires.

Keywords: hydrogen bonds · isomers · pi interactions · supramolecular assembly · tetrathiafulvalene

Introduction

The self-assembly of nanoscopic fibres and rods is an appealing pursuit given that they may form part of molecular electronic devices.[1–3] This bottom-up approach[4–8] to wires offers many advantages over strictly covalent approaches, but one limiting factor is control over the self-assembly process. In this sense, a delicate balance between building block functionality and supramolecular synthons is required.[9]

Apart from the supramolecular design built into the components of these nanometre scale objects, the importance of the deposition method, the solution nature[10–14] and concentration,[15–18] the chain-length dependence,[19–23] and the nature of the surfaces[24–26] on the characteristics of aggregates have been demonstrated for some molecules. To self-assemble wires required for new challenges in molecular electronics, in this work we report the influence of these factors as well as the molecular constitution on hydrogen-bonded assemblies[27–31] of functional π-electron-rich compounds.

The molecules we have chosen for this study are tetrathiafulvalene derivatives (TTFs), because of their great potential in the area of molecular electronics as switches,[32–36] conductors[37,38] and their use in field-effect transistors.[39,40] Our work aims to arrange the TTFs with a close contact in be-

[a] J. Puigmartí-Luis, Dr. Á. Pérez del Pino, Prof. C. Rovira, Dr. D. B. Amabilino
Institut de Ciència de Materials de Barcelona (CSIC)
Campus Universitari de Bellaterra
08193 Cerdanyola del Vallès, Catalonia (Spain)
Fax: (+34) 93-580-5729
E-mail: amabilino@icmab.es

[b] A. Minoia, Prof. R. Lazzaroni
Service de Chimie des Matériaux Nouveaux
Université Mons-Hainaut, Place du Parc 20
7000 Mons (Belgium)

[c] Dr. G. Ujaque, Prof Dr. A. Lledós
Unitat de Química Física
Departament de Química, Edifici Cn
Universitat Autònoma de Barcelona
08193 Bellaterra, Barcelona, Catalonia (Spain)

tween the π surfaces (so that they may be useful for the aforementioned applications) by using hydrogen bonds, and to form nanoscale fibres in a controlled way. In the solid state, hydrogen bonds have been used to influence the disposition of TTF units with varying degrees of success,[41–47] one example being that of amide bonds which aid the formation of stacks of molecules.[48] On the other hand, fibres have been formed in Langmuir films[49,50] and gels[51] with a random orientation, and gels of TTFs have shown some alignment of the fibres.[52] In two cases xerogels based on TTF derivatives have been proven to conduct electricity.[53,54] Here, we show how chemical constitution and composition as well as the surface, solvent of deposition and concentration influence in hydrogen bonded assemblies that the new compounds we report form.

A series of TTF–amide derivatives and other aromatic analogues have been synthesised in order to prove the important role that the amide group plays in forming fibres and rods with nanometre dimensions upon casting them from solution. Two isomers, *cis*- and *trans*-TTF, were targeted to study the effect of the constitution in relation the molecular assembly on a hydrophobic surface.[55] Six different TTF derivatives were studied, three *cis* (**1a**, **1b** and **1c**) and three *trans* (**2a**, **2b** and **2c**), in which the length of the aliphatic

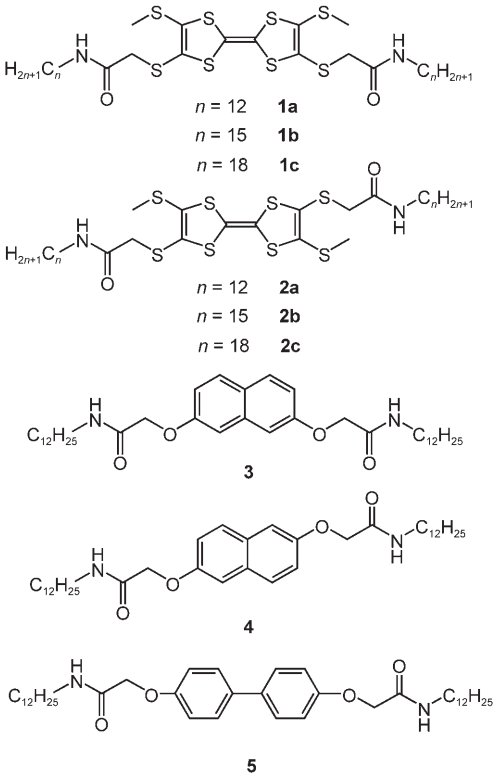

chains were varied. The reason for the different alkyl units was to observe possible effect of chain length and odd–even numbers of carbon atoms on the supramolecular structure. On the other hand, three aliphatic amide substituted aromatic hydrocarbon compounds were studied so that the importance of the TTF unit in the self-assembly process can be evaluated. Two of them are constitutional isomers that have an aromatic core, a naphthalene unit (**3** and **4**), which can form π–π interactions with themselves.[56,57] The last one **5**, does not have a planar core. All of them have amide groups in their structure just to prove the directionality of the hydrogen bond to self-assemble into anisotropic aggregates just casting them from the solution. All the compounds studied include two amide groups, which permit the formation of hydrogen bonds,[58,59] in the case of the TTF as well as short contacts of the sulfur atoms in the residue. In addition, the long alkyl chains can provide a "fastener" effect[60] through dispersion interactions, and can also interact with a graphite surface through van der Waals interactions.

Results and Discussion

Synthesis and characterisation: The TTF–amide derivatives were synthesised starting from thione **6** (Scheme 1).[61] Removal of the protecting propionitrile group with base fol-

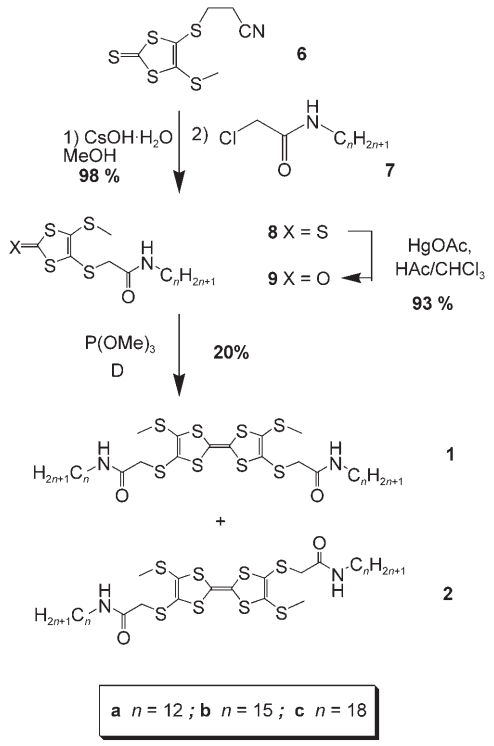

Scheme 1. Synthesis of the TTF constitutional isomers with different alkyl-chain lengths.

lowed by reaction with amides **7** (prepared using a method based on that of Thorsteinsson et al. for **7a**[62]) gave thiones **8**, which in turn were converted into the oxo compounds **9** by treatment with mercury(II) acetate. The self-coupling of these compounds in refluxing trimethylphosphite gave the mixtures of isomers **1** and **2**, which were separated by flash column chromatography. The assignment of the *trans* consti-

tution of the eluted compounds is in accord with previous observations on other isomers of this type,[23,55] and on the ease of crystallization of the two compounds—the *trans* compound **2** crystallises far easier than the corresponding *cis* compound. The compounds were fully characterised by using the usual spectroscopic techniques and elemental analysis (see Experimental Section). The IR spectra of the isomers show the same characteristic band at approximately 3300 cm^{-1}, which is indicative of hydrogen-bonded N–H groups, and the corresponding C=O stretching and N–H bending bands at 1645 and 1551 cm^{-1}, respectively. The ^1H NMR spectra are also very similar, with the amide NH resonances appearing at approximately $\delta = 6.8$ ppm.

Compounds **3**, **4** and **5** were prepared from the commercially available phenols that were treated with **7a** (Scheme 2) with potassium carbonate as the base. The products were purified after filtering the reactant solution and cleaning the solid residue with dichloromethane. They were fully characterized by using the usual spectroscopic techniques as well as elemental analysis.

AFM studies of self-assembled fibres: Solutions of the *trans*-TTF isomers in chloroform were deposited onto highly oriented pyrolytic graphite (HOPG) by simple casting and the solvent was allowed to evaporate. The topography of the nanoscopic solids formed were investigated by atomic force microscope (AFM) by using the acoustic (oscillating tip) mode, in several regions of the surface and in several sessions with different stock solutions and different tips. The images that are presented are the most representative ones for each sample. The compounds form fibres with varying dimensions depending on the concentration of the solutions employed in the casting experiment and the region of the evaporated drop that is studied. The centre of the drop always contained higher concentration of compound.

The AFM images of the aggregates formed from concentrated solutions (10^{-4} M) of **2a** and **2b** in chloroform (Figure 1A and 1B respectively) reveal rodlike objects of varying length and breadth, but with a remarkably consistent orientation. The angle that the rodlike aggregates make with respect to each other in both compounds is: $a = 59 \pm 7°$ and $a = 59 \pm 8°$, respectively. This angle corresponds to the complementary axis angle of the highly oriented pyrolitic graphite (HOPG); so both molecules have an orientation that is determined by this surface, seen previously for completely different systems.[63]

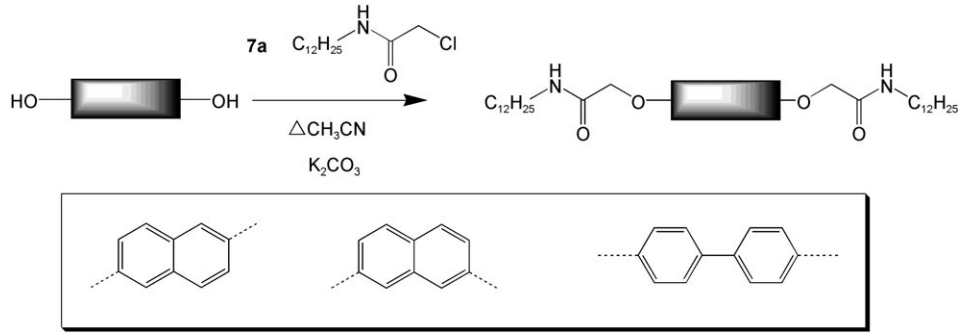

Scheme 2. Synthesis of the aliphatic amides derived from dioxynaphthalenes and biphenol.

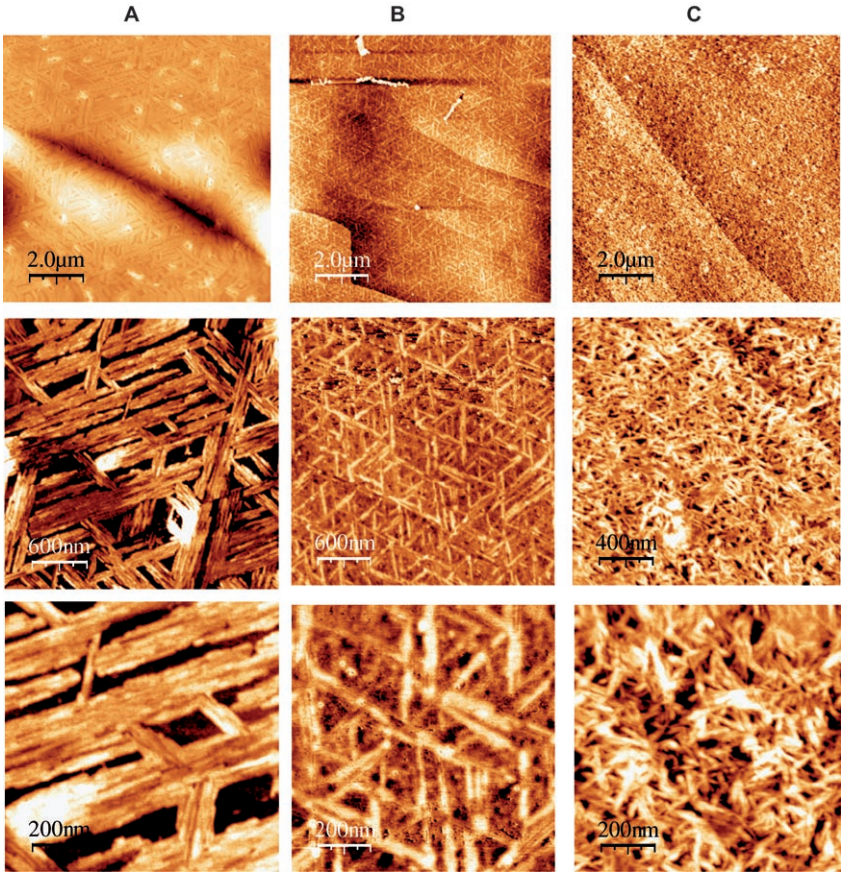

Figure 1. AFM images of A) **2a**, B) **2b** and C) **2c** on HOPG after evaporation of the solvent from 10^{-4} M solutions of the samples in chloroform.

For the *trans*-TTF compound **2a**, the blocklike objects have varying length, but have a quite uniform lateral dimension. The averaged width over different images is 190 ± 73 nm and the height is 3.3 ± 0.6 nm. However, within these aggregates much smaller features are observable (vide infra). In the case of compound **2b** in which the aliphatic chains are longer by three methylene groups, the average dimensions from different images were around 53 ± 17 nm in width and 1.2 ± 0.2 nm in height. In the fibres of this compound too, it is possible to discern small fibres that do not agglomerate as do those of **2a**, and resolution of the individual fibres is more evident.

The lateral dimensions of the aggregates were measured by using the profile from the AFM images (Figure 2). These contours show that the larger fibres formed by **2a** are quite smooth, although very small features can be discerned. The calculated end-to-end distance for a fully-extended molecule of **2a** is 4.7 nm, and that of the core of the TTF (between the sulfur atoms appended to the fulvalene rings) is approximately 0.97 nm. On the other hand, the topographic analysis of the fibres of **2b** on the HOPG shows much better defined and smaller fibres. Individual features less than 10 nm in width and 0.5 nm height indicates that these are fibres composed of single hydrogen-bonded chains of molecules. The calculated distance between the sulfur atoms at either "end" of the TTF unit is approximately 0.9 nm (taking into account tip broadening, an apparent width would be approximately 6 nm). The end-to-end distance for a fully extended molecule of **2b** is 5.5 nm (taking into account the tip broadening, an apparent fibre width would be approximately 15 nm). The features observed therefore point to individually resolved supramolecular fibres.

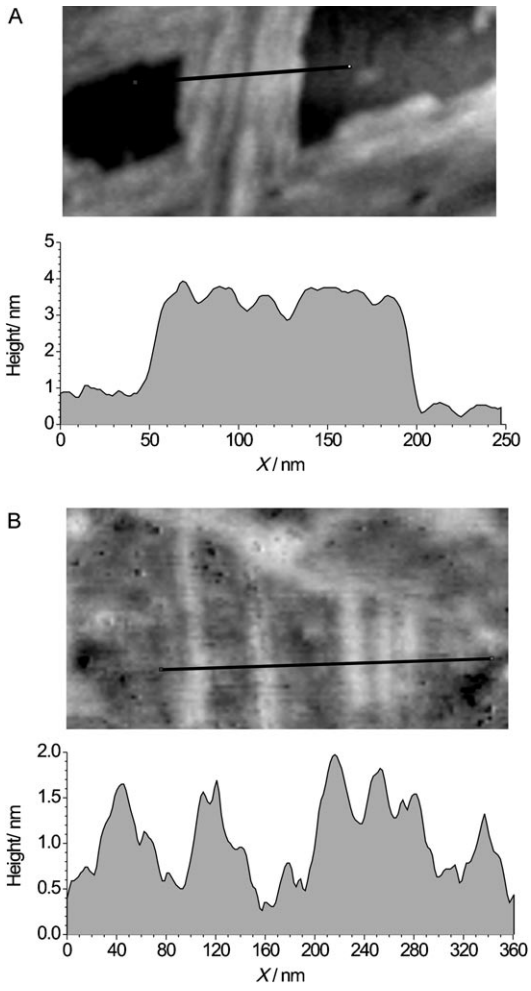

Figure 2. Close-up of AFM images of A) **2a** and B) **2b** on HOPG after evaporation of the solvent from 10^{-4} M solutions of the samples in chloroform, and the corresponding profiles.

The fact that the blocks have such a well-defined size and orientation implies that the surface is certainly aiding as a template during their formation. The different lateral dimensions (especially the observation that the height and width of the aggregates of **2b** are smaller than those of **2a**) could point to the different solubility in the solvent used for deposition, which introduces a kinetic factor into the formation of the self-assembled fibres.

The *trans* isomer **2c** was studied under the same conditions as the homologues with shorter chains. A very different topography is observed in this case. It is characterized by a dense mesh of very fine fibres (width 48 ± 20 nm and height 6.3 ± 2.6 nm) with lengths between 50 and 200 nm. These fibres are randomly distributed over all directions of the surface (Figure 1C). The length of the alkyl chain would not be expected to change the preferred orientation of the hydrogen-bonded assemblies along the principle graphite symmetry axes. Therefore, the small dimensions of the fibres and their random orientation indicate that these nanoscale acicular objects precipitate in solution (rather than on the surface). This hypothesis is supported by the TEM images of the compound away from any surface (vide infra).

Similar casting experiments were carried out to study the influence of the concentration on the supramolecular arrangement of the compounds. Therefore, lower concentration (10^{-5} M) for each *trans* isomer were used. Identical morphologies were observed except for the *trans* isomer **2c**. At 10^{-5} M, this *trans* isomer generates small aggregates and very long isolated fibres (Figure 3). The two types of aggregate have virtually identical height (13.3 ± 0.2 nm) and width (119 ± 2 nm) (Figure 3 right-hand image). This observation makes us hypothesize that the organization of the molecules in the blocks and in the fibres is similar.

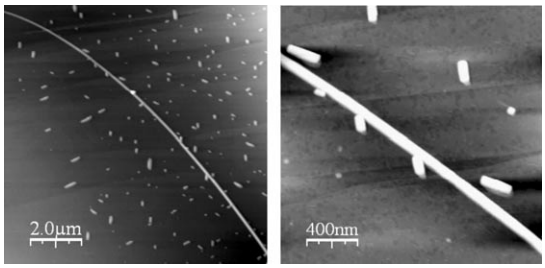

Figure 3. Topographic AFM images of **2c** on HOPG after evaporation of the solvent from a 10^{-5} M solution of the samples in chloroform.

The long aggregates are tens of micrometers in length and are slightly curved on this length scale, although locally they are apparently quite uniform (Figure 3, right-hand image). Working with this lower concentration, it is also possible to generate short aggregates of **2c**, with equal dimensions as described above, which are oriented following the graphite axes ($a = 61 \pm 6°$), as shown in Figure 4. These objects were

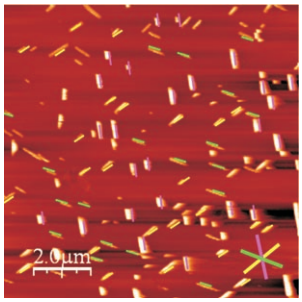

Figure 4. An AFM image of a drop-cast solution (10^{-5} M in chloroform) of compound **2c** on a graphite surface with coloured lines added to show the preferred orientation of the nanorods.

observed in a different area of the surface of the cast material on graphite, although the alignment with the graphite axes can also be seen in the images in Figure 3. The dispersion in the width of the fibres between high and low concentration deposition and the lack of orientation of the fibres for **2c** implies that the ones formed from more concentrated solutions of this compound are deposited under kinetic control rather than under a more thermodynamic influence seen at lower concentrations in chloroform, and in the more general sense for **2a** and **2b**.

However, it is not possible to exclude the possibility that the surface plays some role in the formation of the finer fibres observed in the AFM images of the more concentrated cast solutions of **2c** on graphite.

When the same casting experiments are performed on freshly cleaved mica no fibres or blocks are observed. Instead, mono- and multilayers are observed (Figure 5) along with amorphous chunks of material. Therefore, it appears that the amide derivative's ability to self-assemble is disturbed greatly by the hydrophilic surface, possibly by interaction with the amide groups of the molecule as seen for other amide derivatives.[64]

Solvent has been shown to play an important role on the aggregation of other components which are useful in molecular electronics, for polymers[65,66] and small molecules,[10–14,67] and the same is true here. When solutions of the compounds in tetrahydrofuran were deposited on graphite, films with amorphous character were formed, with no fibril morphology evident (images not shown). When toluene was used to deposit compound **2c** on graphite, no well-defined fibres were formed (as they were in chloroform), but in areas a monolayer was imaged by AFM in which fibril morphology is evident (Figure 6D and E). Within the monolayer small domains with short-range order were

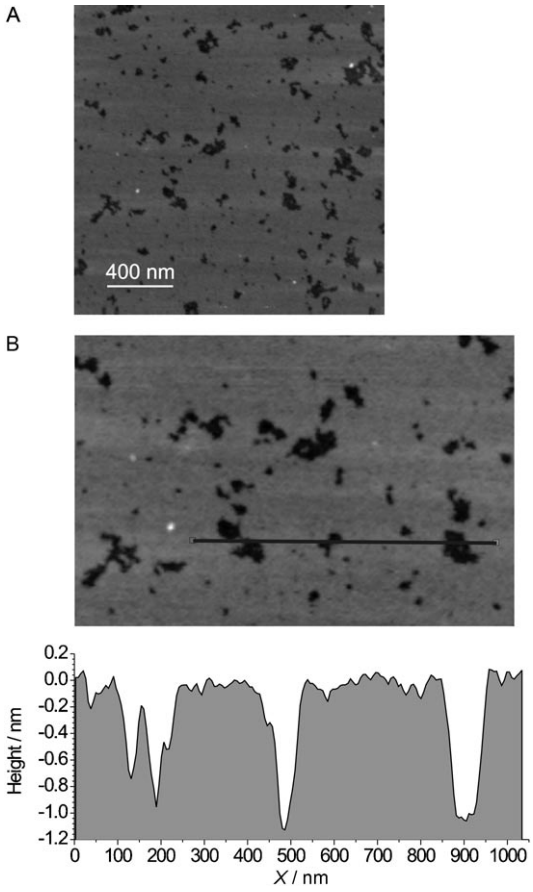

Figure 5. A) An AFM image of a drop-cast solution (10^{-4} M in chloroform) of compound **2c** on a mica surface, showing layer-type morphology, and B) a closer view with the corresponding profile.

formed for which resolution of the individual fibril structures was reached (width 5.5 ± 0.4 nm) by using acoustic mode AFM. The nanodomains are composed mainly of three or four fibres of approximately equal length, indicating that there is some interaction between them, the most likely one being between the alkyl chains by interdigitation. There is no evident alignment of the nanofibres with the graphite axes in these domains (Figure 6D $a = 109 \pm 23°$, Figure 6E $a = 104 \pm 11°$) and these are invariant with the concentration, as is appreciable in Figure 6E.

The constitution of the molecule is also of critical importance. When *cis*-**TTF** derivatives (**1a–c**) were cast onto graphite from toluene or chloroform (at the same concentrations as the *trans* isomers), no well ordered fibres or blocks were observed. Rarely, nanofibres of the type seen for the *trans* isomers (Figures 1 and 6) were observed for the *cis* isomer (Figure 7), but in general the monolayer is far more amorphous than that of the former. Very short fibres which are in close contact were seen for **1a**, while for **1b** longer and wider fibres were seen occasionally, but with no specific orientation in either case. The *cis* compound with the longest alkyl chains (**1c**) forms nanodomains of fibres aligned with each other, rather similar to those of the *trans* compound cast from toluene.

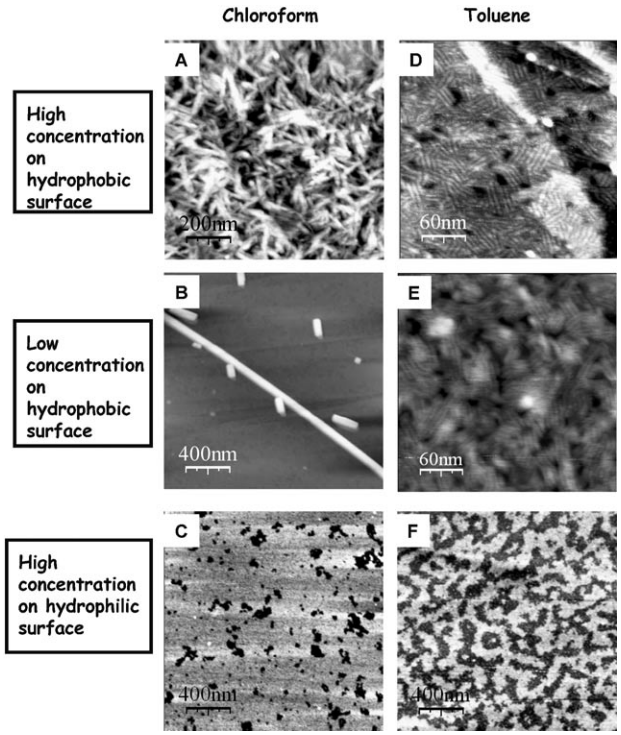

Figure 6. Effects of concentration, solvent and surface type on the morphology of surface-supported aggregates of compound **2c**. The topographic AFM images were recorded for samples on mica (C and F) and graphite (A, B, D and E) surfaces. The high concentration is 10^{-4} M and the low one 10^{-5} M.

These dramatic changes observed in the topography as a result of the molecular constitution makes us hypothesize that in the case of the *cis* isomers smaller fibril structures are observed because of the stronger interaction of the TTF derivatives with the surface. Both alkyl chains of these *cis* isomers can bond with the surface through van der Waals interactions, making short and small fibril-containing domains, while for the *trans* isomers the contact of both chains is less favourable because of their S shape (as seen perpendicular to the plane of the molecule).

The hypothesis described above is in total agreement with the experimental data obtained from averaged measurements of the different *cis*-TTF derivative AFM images. Their aggregate dimensions never exceed those of the *trans* derivatives (Figure 8). The size of the fibril structures imaged for the *cis* isomers (**1a** and **1c**) are consistent with the molecular dimensions (width 6–7 nm and height between 0.2–0.4 nm). For the *trans* isomer hierarchical supramolecular interactions are possible because this constitution allows one of the chains to be lifted up from the surface and this can interact with other molecules making the surface less influential in the aggregate formation than for the *cis* isomers. The relative surface independence is exemplified for **2c** at the higher concentration studied.

A parallel study was carried out with the different amide derivatives **3**–**5** that do not contain the TTF unit, but rather aromatic hydrocarbon groups. The aim of this investigation

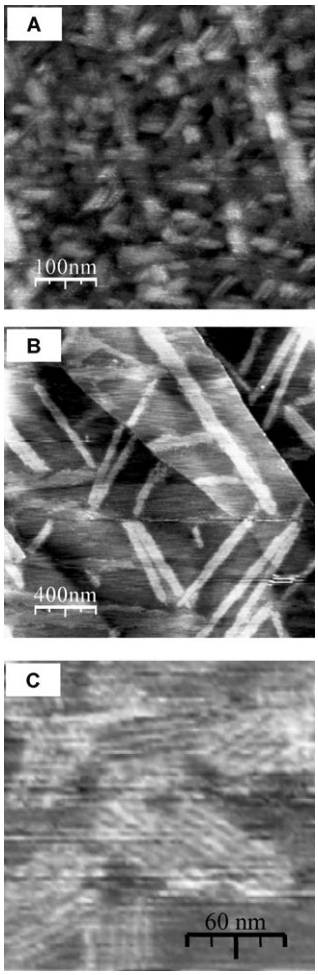

Figure 7. AFM images of cast layers of A) **1a**, B) **1b** and C) **1c** from 10^{-4} M solutions of the samples in chloroform on HOPG.

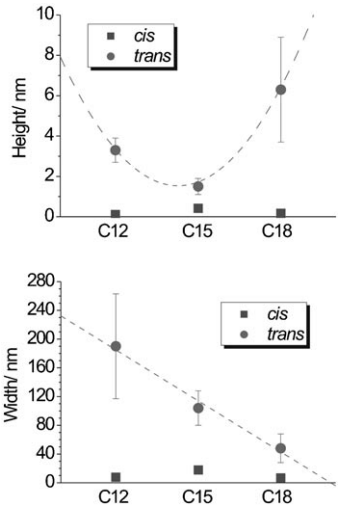

Figure 8. Graphs showing the average dimensions of the fibre-like objects of the TTF derivatives **1** and **2** observed from different images and samples.

was to evaluate the relative importance of the hydrogen bond in the fibre formation, and the role of the planar core (in **3** and **4**) with π–π interaction ability or the nonplanar core (**5**) on the supramolecular assembly. Two molecules with a planar naphthalene core (**3** and **4**), and the other with a more conformationally flexible biphenyl core (**5**) were deposited onto the graphite in the same way as for the TTF derivatives. All them have two possible hydrogen-bond centres and dodecyl chains, and so can be compared with **1a** and **2a**. The 2,7-naphthyl derivative **3** is comparable in its constitution to the *cis*-TTF derivative **1a**, while the 2,6-naphthyl derivative **4** is similar to the *trans* isomer **2a**, and this fact is reflected to some extent in the type of aggregates that they form (vide infra).

The type of self-assembled structure observed for **3**, **4** and **5** on graphite depends strongly on the amount of material deposited on the surface (determined by the local concentration during evaporation of the solvent) in the area being imaged (Figure 9). Comparison of the AFM images of molecules **3** and **4** shows the important role that constitution has in the self-organization with respect to the surface. For compound **3** (Figure 9A) a dense mesh of thin fibres, which have no strict alignment with the graphite axes, is observed. This kind of supramolecular assembly was also seen for the *cis* isomer **1c**, but the uniform areas were not as large and the definition of the fibres was nowhere near as high as in the present case. This type of aggregate seems characteristic of a strong interaction between the alkyl chains of the molecule and the surface, thanks to the location of these chains on the same "side" of the aromatic rings. The small fibrils are of molecular dimensions (width 4.8 ± 1.1 nm and height 0.13 ± 0.03 nm, Figure 10). There is also evidence of larger fibres for compound **3**, something not seen for compounds **1**. This evidence indicates a stronger molecule–molecule interaction in the naphthalene derivative than in the TTF compound. The images of compound **4** (Figure 9B) also reveal the formation of fibril-like structures, but with much larger dimensions (width 152 ± 25 nm and height 17.6 ± 1.7 nm, Figure 9Bi) similar, but much larger than those formed by **2a**, which has a similar molecular constitution. Also, areas that appear to be uniform mono- and multilayers are formed on the graphite surface. Again, then, the AFM

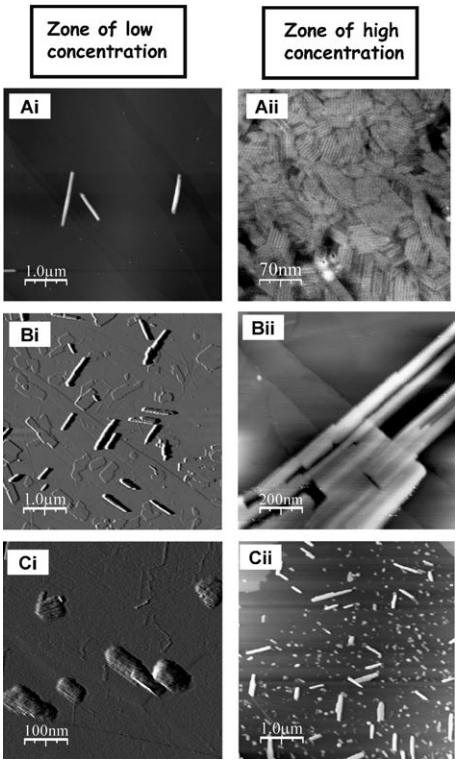

Figure 9. AFM images of 10^{-4} M solutions of compounds A) **3**, B) **4** and C) **5** in chloroform after evaporation of the solvent after casting on graphite. All images show the topography signal except Bii and Cii, which show the phase shift of the oscillation of the AFM tip in order to show the fine structure more clearly.

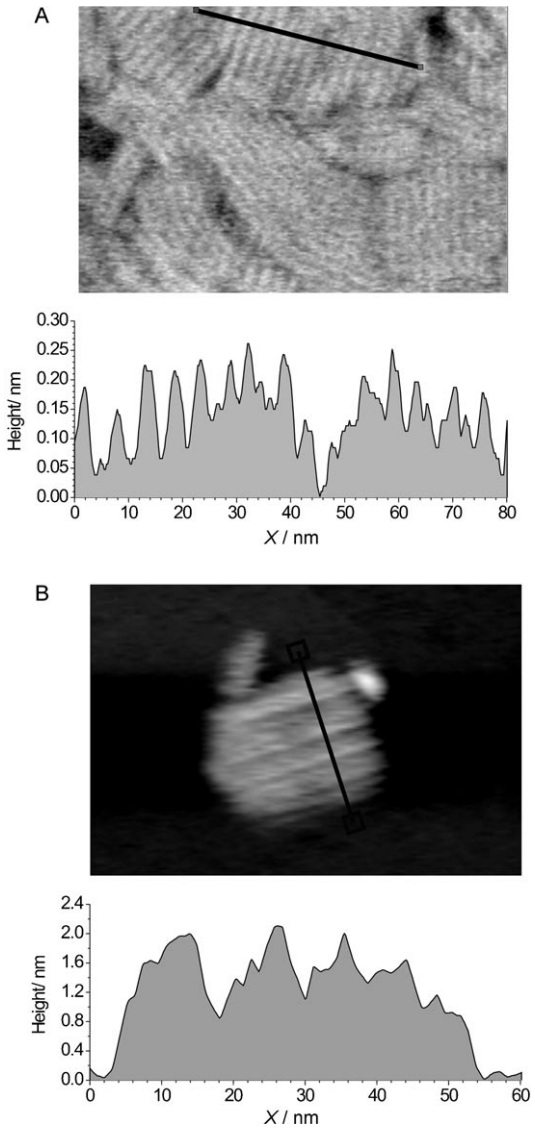

Figure 10. Profiles from the AFM images of cast samples of compounds A) **3** and B) **5** on HOPG.

evidence points to stronger molecule–molecule interactions in the naphthalene derivative than in the TTF derivative.

Images of compound **5** on graphite (Figure 9C) show areas of monolayer (top left in Ci) and rodlike aggregates. As in the case of the TTF derived compounds **2**, these aggregates are aligned with the graphite symmetry axes. The oblong objects also have internal fibril structure, as shown the phase image in Figure 9Cii. Therefore, we can conclude that a planar molecular centre is not essential to achieve the fibrelike aggregates, although it does influence greatly their dimensions and morphology.

Current sensing AFM Studies of self-assembled fibres: After studying the supramolecular arrangement of the different amide derivatives on graphite, we chose to study the electrical properties of a conducting film on graphite prepared by doping compound **2c** on the substrate. We used compound **2c**, because it is the one material which forms a mesh of fibres, and close contacts between crystals have been shown to be important for conductivity in films of larger crystals of TTF salts.[68,69] The film was prepared with a concentrated solution of neutral **2c** (10^{-4} M) after casting it several times onto graphite to give a film of up to 300 nm in thickness, with the same morphology as thinner films. The material was doped by exposure to iodine vapour for two minutes, which generates the cation radical of the π donor while leaving some in the neutral state. This mixed valence material was studied with current sensing AFM, a technique which has proven useful in the characterization of covalent polymer systems.[70,71]

Several current images were recorded by applying a bias voltage to the sample while scanning with a grounded conducting tip. Current maps were obtained where fibre structure arising from the differences in electronic transport in the film can be observed clearly (Figures 11 and 12). This

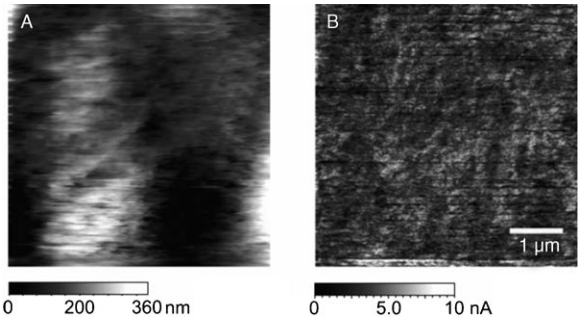

Figure 11. A) Topographic and B) current image (0.1 V bias) of an iodine-doped sample of **2c** on HOPG.

detail was not discernable in the topographic images which were acquired simultaneously. This result implies that the current is flowing along the stacked TTF moieties in the supramolecular wires.

The spectroscopy (*I* versus *V*) curves obtained in different areas of the sample show metallic character clearly, with a

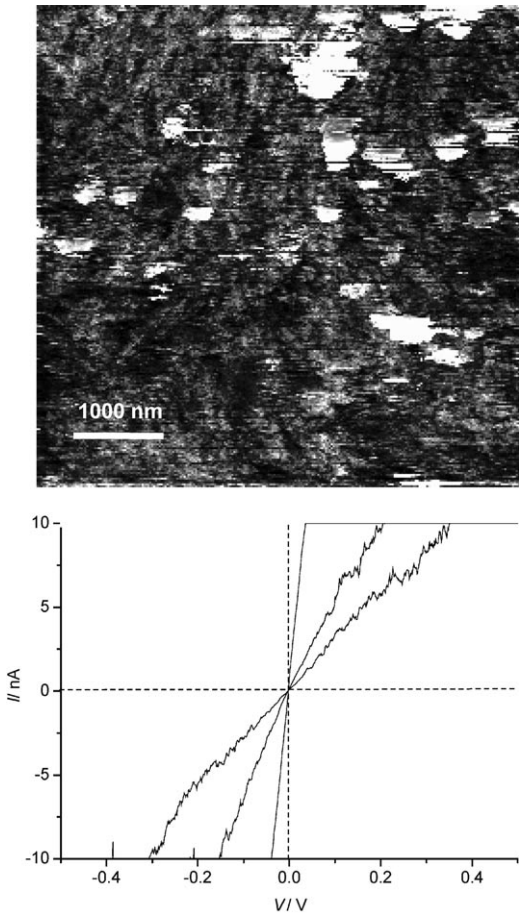

Figure 12. Current map of a doped film of compound **2c** on graphite and *I/V* curves taken at different locations in the current maps.

different slope according to the zone (Figure 12). The dispersion in the slope of the *I/V* curves and the appearance of the current map over the whole sample is essentially negligible. A representative selection of averaged spectroscopy curves is shown in Figure 12. The most inclined curve was observed in areas with higher current, and is associated with a resistance of 7.5 MΩ. The curve with intermediate slope, corresponding to an area of intermediate conductivity, had a resistance of 18.0 MΩ. The zones where the current is lowest had a resistance of 33.0 MΩ, but still showed metallic characteristic, that is, no experimental gap was observed. These data correspond well with the resistance obtained from the statistical calculations done on the current sensing images. These calculations consisted of obtaining the current value which was most probable from the current distribution, which gave a value of 4.5 nA. This current would imply a resistance of 25.0 MΩ (far greater than the tip resistance, of approximately 1 kΩ) for the map generated at 0.1 V.

TEM studies of self-assembled fibres: When the molecule–molecule interactions are sufficiently strong, it should be possible to obtain fibril-like aggregates of nanoscopic size and acicular shape. To evaluate the influence of the surface in the aggregate assembly of the compounds reported here,

we studied the amide derivatives by using a technique which allows observation of the aggregates away from the surface: Transmission electron microscopy (TEM) was used, depositing the compounds from chloroform solutions onto carbon coated copper grids. The samples were not coated with any contrast agent, and the images were recorded at room temperature.

The images confirm the tendency of *trans* conformers to form fibrelike structures. Representative examples of the anisotropic objects are shown in Figure 13. The fibres, which

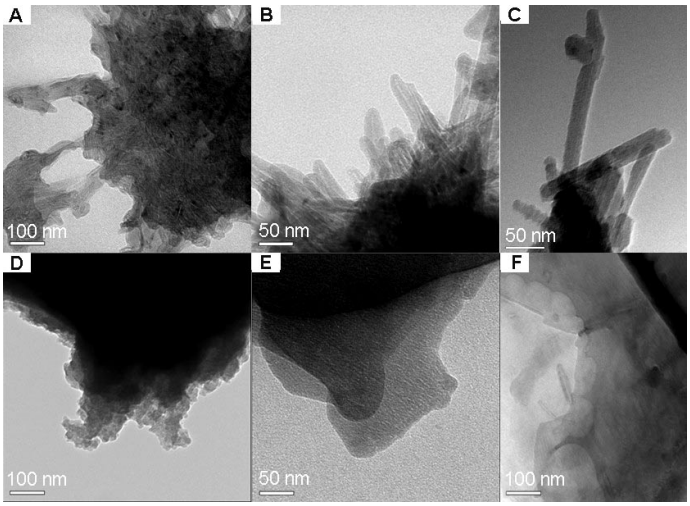

Figure 13. TEM images of the aggregates formed by compounds A) **2a**, B) **2b**, C) **2c**, D) **1a**, E) **1b** and F) **1c** after evaporation of the solvent from 10^{-4} M solutions of the samples in chloroform on the carbon-coated copper grid.

are approximately 20–40 nm wide and several hundreds of nanometres long, have internal structure that corresponds to the length of the molecules, 5–6 nm. This study confirms the inherent capacity of the *trans* molecules to form fibres from a solution of the sample in chloroform and bears witness to the strong molecule–molecule interactions that take place while the solvent evaporates from the solutions. The fact that the most well-defined fibres are seen for **2c** explains the observation of the fibres on the graphite surface without any orientation with respect to the substrate: They presumably precipitate from solution before growth from adsorbed molecules on the surface can take place.

In case of the *cis* conformers, the behaviour is different. The compounds **1** cannot form fibril-like aggregates without surface influence (Figure 13D, E and F).

The TEM study of the other amide derivatives (**3**–**5**) which do not contain the TTF unit, confirms the strong interaction only between molecules of **3**. In Figure 14 the TEM images of this compound are shown in which fibrous texture can be discerned. Compounds **4** and **5** do not show the same surface independence of fibre formation, only amorphous material was observed in the TEM experiments (images not shown). The molecular constitution therefore

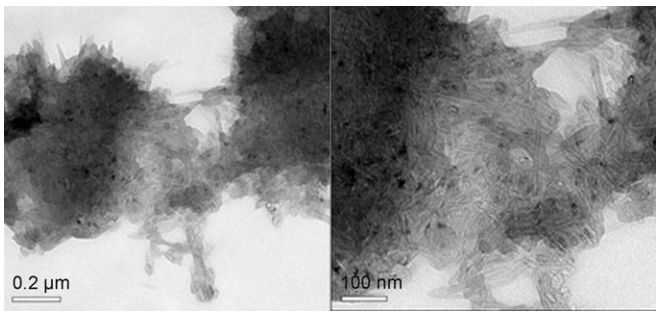

Figure 14. TEM images of compound **3** after evaporation of the solvent from a 10^{-4} M solution of the sample in chloroform on the holey carbon grid.

has a profound influence on the supramolecular structures that are formed through hydrogen bonds.

Simulation of aggregate formation—the role of interactions in columnar stacks: To study the influence of hydrogen bonds in self-assembly of TTF derivatives with a tractable computational effort, the compounds **1** and **2**, in which a methyl group is the substituent at the nitrogen atom, have been modelled with force field (FF) techniques. The most likely conformers have been identified with Monte Carlo (MC) conformational analysis (see Computational Methods for details). Then stacks of eight molecules were built, their structure optimized with molecular mechanics (MM) and the final energy evaluated. Each structure is composed of only one conformer of the molecule, all with the same orientations in space and relative positions, because it is clear that the high order observed experimentally in the aggregates must arise from a high regularity at the molecular level. The final structures of the aggregates are strongly influenced by the type of interaction that starts to act between the molecules, as the stack is formed independently from the order in the stack.

Figures 15A and 16A show two different initial structures for the *trans*-TTF isomer: In the first one, the TTF parts of the molecules are approximately 7 Å distant, while in the second one the intermolecular distances are less than 4 Å. When the molecules are far from each other, as in Figure 15A, the intermolecular interactions have a dipole–dipole nature, while π–π interactions and hydrogen bonds act only when the molecules get close to each other. The dipole–dipole forces induce a misalignment of the molecules and the resulting structure (Figure 15B) is quite disordered and is not consistent with what is observed experimentally.

Instead, when molecules are close to each other, as in Figure 16A, and the intermolecular distances are comparable to the range of action for π–π interactions, the resulting structure (Figure 16B) maintains the initial regular packing. Figure 16 shows the initial structure in which the molecules of the *trans*-TTF derivative are closely packed (A) and the resultant optimized structure (B). Here π–π interactions already act in the starting geometry keeping the molecules

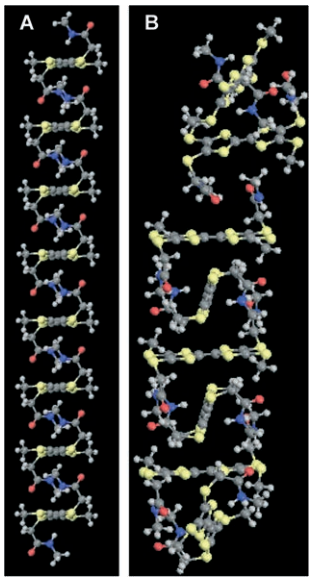

Figure 15. A) Initial structure of the *trans*-TTF compound in which the molecules are 6–7 Å apart. B) Optimized geometry: the disorder is due to the dipole–dipole interactions, which act on a longer scale with respect hydrogen-bond and π–π interactions.

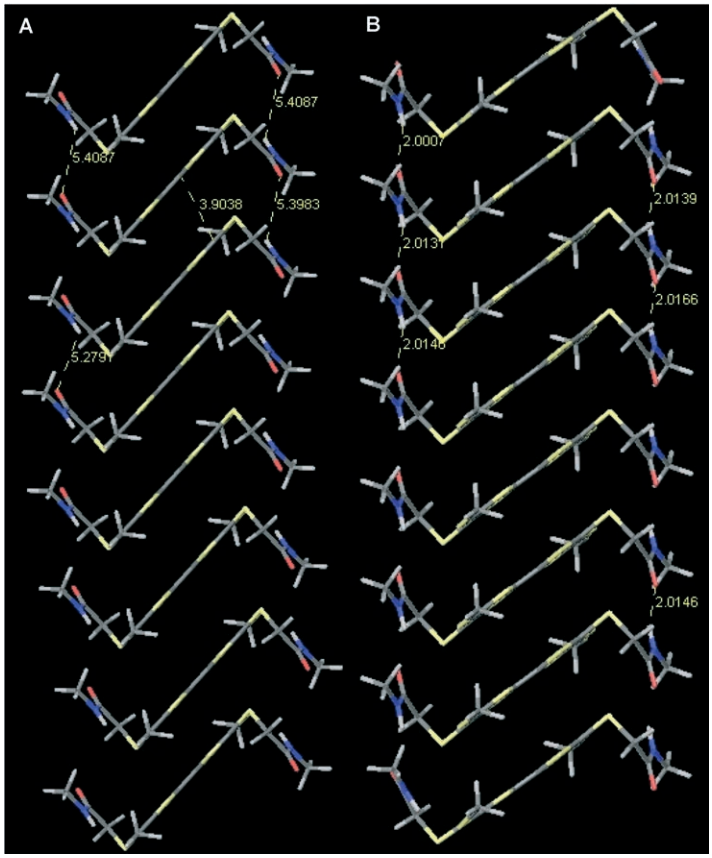

Figure 16. A) Initial structure in which the molecules of the *trans*-TTF derivative are closely packed and B) the resultant optimized structure.

aligned together. The effect of the minimization is the formation of the hydrogen bonds, which strongly bind the molecules to each other. It is important to notice that, with respect to the real case, here there is no surface to force the molecules into a particular alignment, so we can also observe other structures such as the helical aggregate shown in Figure 17.

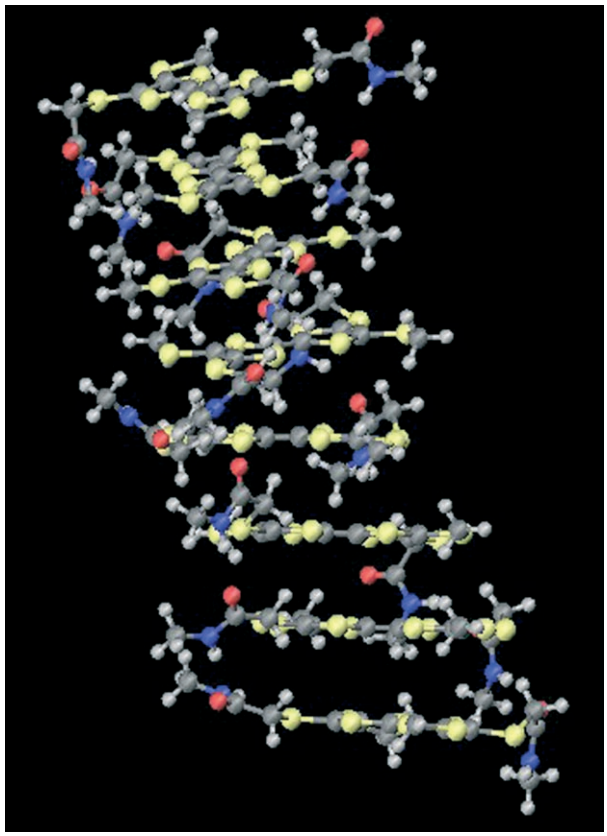

Figure 17. Optimised helical structure: this is the most stable stack in absence of a surface.

Seven different structures, which show a well ordered packing (compatible with assembly on a surface or that observed in the TEM measurements), have been studied and all are within 13 kcal mol^{-1} in absolute energy. We have also examined the molecular binding energy in those structures, as defined in Equation (1), which is possibly more significant than the absolute energy for the stacks, because it represents the gain in energy for an isolated molecule when incorporated in the structure.

$$E_{\mathrm{bind}} = \frac{E_{\mathrm{abs}}^{\mathrm{stack}} - (N_{\mathrm{mol}}\, E_{\mathrm{min}}^{\mathrm{isol}})}{N_{\mathrm{mol}}} \qquad (1)$$

In Equation (1), $E_{\mathrm{abs}}^{\mathrm{stack}}$ is the energy of the stack, N_{mol} is the number of molecules in the stack and $E_{\mathrm{min}}^{\mathrm{isol}}$ is the energy of the most stable conformer for the isolated molecule, obtained by Monte Carlo conformer search. All the binding energies calculated for the structures analysed (Table 1) are quite close, so it is not possible to identify a structure that is clearly the most stable.

Table 1. Binding energy (E_{bind} in kcal mol^{-1} per molecule) of molecular packing.

Configuration	E_{bind}	Configuration	E_{bind}
cis	−22.7	*trans*	−22.9
cis	−22.0	*trans*	−24.0
cis	−23.9	*trans*	−22.4
cis	−23.3		

The calculations also show that the two amide groups in the TTF derivatives under study, as well as the π–π interactions between the conjugated cores, are needed for the formation of stable aggregates. These groups are, in fact, the active sites for the formation of the hydrogen bonds that strongly bind the molecules to each other. Furthermore, while stable aggregates can be obtained with both *cis* and *trans* conformers modelled, the most ordered are those formed by the *trans* derivatives, consistent with the AFM results. This can be explained in terms of stacking capabilities of the two isomers. Two molecules arrange so as to maximize the number of intermolecular interactions, as shown by MM optimization: *cis* molecules tend to form a "closed shell" using all the amide groups to form hydrogen bonds, as shown in Figure 18. This leads to a "building block" with

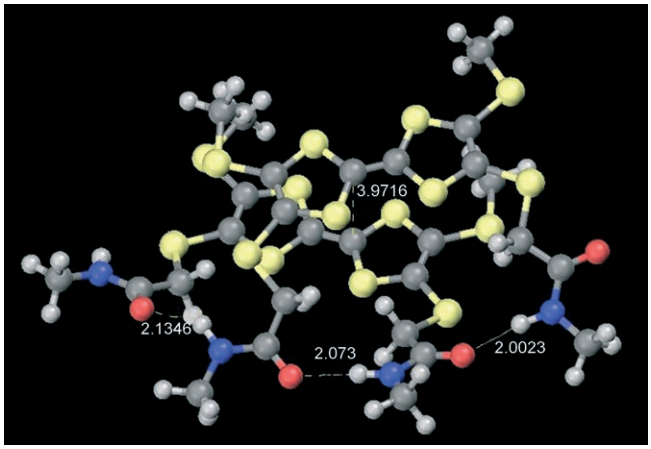

Figure 18. Representation of the *cis–cis* dimer, in which the maximum number of hydrogen bonds is formed between the two molecules.

poor stacking capabilities, which can introduce disorder in the supramolecular structure. In contrast, for *trans* molecules the "building block" has better stacking capabilities, since two amide groups on each side of the supramolecule are still available to bind other units in a "columnar" geometry, leading to a well-ordered, close-packed situation.

Conclusion

Nanometre-scale fibres containing π-electron-rich units can be favoured by employing the amide group as a noncovalent assemble; the use of this group has proven to be an extremely useful tool for their generation on and off surfaces thanks to intermolecular hydrogen bonds. The formation of these fibres is sensitive to solvent, surface, and constitution and composition of the molecule, but it is controllable.

Graphite clearly plays a role in orienting them in some cases and in certain conditions under which the surface–molecule interactions are able to organize the aggregates. In the cases in which molecule–molecule interactions are strong in the evaporating solution, the fibres are non-oriented, as in the case of **2c** and the naphthalene derivatives **3** and **4**. The different sizes of the aggregates observed on graphite are influenced by the local concentration of the molecules in the evaporating solution. Kinetics is clearly an important factor in this crystallization process at the surface, but the thermodynamics of the interaction between the molecules and the graphite also plays a key role in the self-assembly process.

The constitution of the molecules is very important, the *transoid* have a clear advantage over *cisoid* forms of the molecules, because the two hydrogen bonds that are formed favour an additional stabilizing interaction for the aggregates between the aromatic groups as shown by the theoretical studies. The *cisoid*-type molecules apparently interact more favourably with the surface, and modelling indicates that dimerisation of the molecules could act as a barrier to growth of the chains. The length of the alkyl chains attached to the secondary amide also influence the size of the aggregates, longer alkyl chains giving rise to the formation of longer, thinner fibres.

The TTFs reported here are promising components for molecular electronics as indicated by the current sensing AFM studies, which show metallic-type behaviour when doped chemically on the graphite surface.

Experimental Section

General methods and materials: IR spectra were recorded on a Fourier transform Perkin–Elmer, Spectrum One spectrometer; the samples were dispersed in KBr pellets. ^{1}H NMR and ^{13}C NMR were recorded with a Bruker Avance 250. Tetramethylsilane or residual solvent protons were used as internal standard. Laser desorption ionization time-of-flight (LDI-TOF) mass spectra were recorded on a Maldi2 K-probe (KRATOS ANALYTICAL) mass spectrometer. The spectra were recorded by using pulsed extraction of positive ions and with high power (20 kV). Samples were deposited onto the stainless steel sample plates from chloroform. The atomic force microscopy (AFM) images were recorded on a PicoSPM (Molecular Imaging). The acoustic mode was used with resonance frequencies of the silicon tips (Nanosensors, FM type force constant 1.2–3.5 N m^{-1} and diameter 5 nm) of around 60–70 kHz. All the images were recorded under atmospheric conditions. The current images were recorded in contact mode with a bias voltage applied to the sample, while scanning with a grounded conducting Pt–Ir coated silicon tip (force constant around 1.2 N m^{-1}). The graphite used was highly oriented pyrolytic graphite (HOPG), ZYB quality, 12 × 12 × 2 mm^3, GE Advanced Ceramics. The transmission electron microscopy (TEM) was performed by using a Hitachi 800 MT microscope with a Multiscan camera from Gatan. The grids used were carbon-coated copper grids from Monocomp. The melting points were recorded by using a Perkin–Elmer DSC7 differential scanning calorimeter with 25 μL aluminium pans. To check the purity of the compounds analytical TLC (silica 60 F_{254} (Merck) on aluminium foil) were carried out. Flash column chromatography was carried out on silica

(35–70 μm (from SDS)). The solvents used during the synthesis were distilled using standard methods. In particular, THF was distilled from sodium benzophenone ketal under nitrogen atmosphere and $P(OMe)_3$ was distilled in vacuo from sodium metal. Dichloromethane, chloroform and acetonitrile were distilled from phosphorous pentoxide under an inert atmosphere. Compound **6** was synthesised according to a known method.[61]

Computational methods: Several aggregates (dimers, stacks) were simulated using the molecular modeling package TINKER 4.2.[72] Molecular mechanics (MM) calculations were performed with the MM3 FF available in the TINKER package. This force field was chosen because it takes explicitly into account directional hydrogen bonds and provides a reliable description of π-systems.

Monte Carlo (MC) simulations were used to find the most likely conformers for single molecules of the modelled compounds (with the long alkyl groups replaced by methyl groups) at room temperature. Seven conformers, both *cis* and *trans*, within 3 kcal mol^{-1} with respect the most stable one were identified and used to model aggregates.

***N*-Dodecyl-2-chloroacetamide (7a)**: This method was similar to that described by Thorsteinsson et al.[62] with minor modifications. Chloroacetyl chloride (4.4 mL, 55 mmol) and *N*-*N*- dimethyl-4-aminopyridine (0.1 mg) were dissolved in dichloromethane (50 mL). This solution was cooled to 0 °C and dodecylamine (9.30 g, 50 mmols) with triethylamine (8.4 mL) in dichloromethane (10 mL) was added dropwise over one hour. The resulting solution was stirred for a further three hours at room temperature. The solvent residue was filtered and the filtrate was treated with HCl (1 M), by extraction (3×15 mL). The resulting organic phase was dried using $MgSO_4$. Finally, the organic solvent was filtered and evaporated to give 8.40 g of a white solid (65 %). M.p. 61.9 °C; FT-IR: $\tilde{\nu}$ = 3299 (m, NH), 2955 (s), 2917 (s), 2872 (s), 2848 (s), 1670 (s, CCONH), 1644 (s, CONH), 1549 (m, CONH), 1518 (m, C=O), 1468 (m), 1400 (w), 1264 (w), 1234 (w, C–N), 1071 (w), 928 (w), 835 (w), 786 (w), 721 (w, NH), 617 cm^{-1} (w); ^{1}H NMR (250 MHz, $CDCl_3$): δ = 6.61 (s, 1H; -NH), 4.07 (s, 2H; ClCH_2CO-), 3.32 (q, J = 6.9 Hz, 2H; - NHCH_2-), 1.5–1.2 (m, 20H; -NHCH$_2$(CH_2)$_{10}$CH$_3$), 0.89 ppm (t, J = 6.4 Hz, 3H; -(CH$_2$)$_{10}$CH_3); ^{13}C NMR (62.8 MHz, $CDCl_3$): δ = 165.4 (-*C*ONH-), 42.4 (*C*H$_2$Cl), 39.6 (-NH*C*H$_2$CH$_2$-), 31.6, 29.3, 29.2, 29.2, 29.0, 28.9, 26.5, 22.4 (-NHCH$_2$-(*C*H$_2$)$_{10}$CH$_3$), 13.8 ppm (-NH(CH$_2$)$_{11}$*C*H$_3$); elemental analysis calcd (%) for $C_{14}H_{28}ClNO$: C 64.22, H 10.78, N 5.35; found: C 64.33, H 10.66, N 5.26.

***N*-Pentadecyl-2-chloroacetamide (7b)**: The method used was that described for **7a**, in which chloroacetyl chloride (0.9 mL, 11 mmol) and pentadecylamine (3.12 g, 13.7 mmol) were reacted together. Compound **7b** was isolated as a white solid (2.25 g, 54 %). M.p. 68.7 °C; FT-IR: $\tilde{\nu}$ = 3307 (m, NH), 2956 (s), 2922 (s), 2852 (s), 1737 (s, CONH), 1655 (s, CONH), 1548 (m, CONH), 1464 (m), 1452 (m), 1354 (w), 1317 (w), 1212 (s, C–N), 1178 (w), 1143 (w), 786 (w), 720 cm^{-1} (w, NH); ^{1}H NMR (250 MHz, $CDCl_3$): δ = 6.58 (s, 1H; -NH), 4.04 (s, 2H; ClCH_2CO-), 3.29 (q, J = 7.0 Hz, 2H; -NHCH_2(CH$_2$)$_{13}$CH$_3$), 1.5–1.2 (m, 26H; -ClCH$_2$CONHCH$_2$(CH_2)$_{13}$CH$_3$), 0.89 ppm (t, J = 6.4 Hz,3H; -(CH$_2$)$_{13}$CH_3); ^{13}C NMR (62.8 MHz, $CDCl_3$): δ = 165.4 (-*C*ONH-), 42.4 (*C*H$_2$Cl), 39.6 (-NH*C*H$_2$CH$_2$-), 31.6, 29.4, 29.4, 29.3, 29.3, 29.2, 29.0, 29.0, 28.9, 26.5, 22.4 (-NHCH$_2$(*C*H$_2$)$_{13}$CH$_3$), 13.8 ppm (-NH(CH$_2$)$_{14}$*C*H$_3$); elemental analysis calcd (%) for $C_{17}H_{34}ClNO$: C 67.18, H 11.28, N 4.61; found: C 67.24, H 11.36, N 4.59.

***N*-Octadecyl-2-chloroacetamide (7c)**: The method used was that described for **7a**, in which chloroacetyl chloride (2.0 mL, 25 mmol) and octadecylamine (8.12 g, 30 mmol) were reacted together, giving **7c** as a white solid (5.31 g, 51 %). M.p. 76.9 °C; FT-IR: $\tilde{\nu}$ = 3292 (m, NH), 2954 (s), 2916 (s), 2848 (s), 1666 (s, CONH), 1645 (s, CONH), 1551 (m, CONH), 1468 (m), 1415 (w), 1375 (w), 1301 (w), 1264 (w, C–N), 1233 (w), 1161 (w), 720 cm^{-1} (w, NH); ^{1}H NMR (250 MHz, $CDCl_3$): δ = 6.57 (s, 1H; -NH), 4.04 (s, 2H; ClCH_2CO-), 3.30 (q, J = 6.7 Hz, 2H; -NHCH_2-(CH$_2$)$_{16}$CH$_3$), 1.5–1.2 (m, 32H; -ClCH$_2$CONHCH$_2$(CH_2)$_{16}$CH$_3$), 0.88 ppm (t, J = 6.2 Hz, 3H; -(CH$_2$)$_{16}$CH_3); ^{13}C NMR (62.8 MHz, $CDCl_3$): δ = 165.4 (-*C*ONH-), 42.4 (*C*H$_2$Cl), 39.6 (-NH*C*H$_2$CH$_2$-), 31.6, 29.4, 29.3, 29.2, 29.0, 29.0, 28.9, 26.5, 22.4 (-NHCH$_2$(*C*H$_2$)$_{16}$CH$_3$), 13.8 ppm (-NH(CH$_2$)$_{17}$*C*H$_3$); elemental analysis calcd (%) for $C_{20}H_{40}ClNO$: C 69.43, H 11.65, N 4.05; found: C 69.54, H 11.55, N 3.97.

4-Thioacetododecylamido-5-methylthio-1,3-dithiol-2-thione (8a): $CsOH·H_2O$ (0.95 g, 5.66 mmol) in MeOH (8 mL) was added over a period of 30 min to a solution of **6** (1.53 g, 5.65 mmol) in CH_3CN/THF (1:1, 60 mL) under Ar and with vigorous stirring. The resulting mixture was stirred for a further 30 min, then **7a** (2.51 g, 9.59 mmol) and a small amount of NaI were added and the solution was heated at reflux for 5 h. The organic solvent was filtered while hot to remove a white solid (which was discarded) and the solution was evaporated to dryness in vacuo. The resulting oily material was purified by flash column chromatography on silica gel ($CHCl_3$/EtOAc; 99:1) to give **8a** in 98 % yield (2.30 g) as a yellow powder. M.p. 76.4 °C; FT-IR: $\tilde{\nu}$ = 3296 (m, NH), 2955 (s), 2919 (s), 2849 (s), 1637 (s, CONH), 1545 (s, CONH), 1462 (w), 1401 (w), 1317 (w), 1264 (w, C–N), 1234 (w), 1056 (m, C=S), 1032 (w), 920 (w), 721 cm^{-1} (w, NH); ^{1}H NMR (250 MHz, $CDCl_3$): δ = 6.53 (s, 1H; -SCH$_2$CON*H*-), 3.56 (s, 2H; -SCH_2CO-), 3.32 (q, J = 7 Hz, 2H; -CONHCH_2(CH$_2$)$_{10}$CH$_3$), 2.57 (s, 3H; -SCH_3), 1.29 (m, 20H; -CONHCH$_2$(CH_2)$_{10}$CH$_3$), 0.91 ppm (t, J = 6.2 Hz, 3H; -CONHCH$_2$(CH$_2$)$_{10}$CH_3; ^{13}C NMR (62.8 MHz, $CDCl_3$): δ = 209.6 (-*C*=S), 165.9 (-*C*ONH-), 128.8 (-C=C-), 39.9 (-NH*C*H$_2$CH$_2$-), 39.4 (-S*C*H$_2$CONH-), 31.6, 29.4, 29.3, 29.2, 29.2, 29.0, 26.7, 22.4 (-NHCH$_2$-(*C*H$_2$)$_{10}$CH$_3$), 19.0 (-S-*C*H$_3$), 13.8 ppm (-NH(CH$_2$)$_{11}$*C*H$_3$); elemental analysis calcd (%) for $C_{18}H_{31}NOS_5$: C 49.38, H 7.14, N 3.20; found: C 49.13, H 7.72, N. 3.83.

4-(Thioacetopentadecylamido)-5-methylthio-1,3-dithiol-2-thione (8b): The procedure was the same as that described for **8a**, with **6** (1.40 g, 5.27 mmol), $CsOH·H_2O$ (0.90 g, 5.35 mmol) and of **7b** (2.35 g, 7.73 mmol). The eluent for the column chromatography was $CHCl_3$/EtOAc 95:5. Finally 1.95 g (77 %) of **8b** was isolated. M.p. 84.3 °C; FT-IR: $\tilde{\nu}$ = 3287 (m, NH), 2954 (s), 2919 (s), 2848 (s), 1634 (s, CONH), 1546 (s, CONH), 1460 (w), 1417 (w), 1400 (w), 1316 (w), 1262 (w, C–N), 1199 (w), 1131 (w), 1057 (m, C=S), 902 (w), 722 cm^{-1} (w, NH); ^{1}H NMR (250 MHz, $CDCl_3$): δ = 6.49 (s, 1H; -SCH$_2$CON*H*-), 3.54 (s, 2H; -SCH_2CO-), 3.29 (q, J = 6.7 Hz, 2H; -CONHCH_2(CH$_2$)$_{13}$CH$_3$), 2.54 (s, 3H; -SCH_3), 1.26 (m, 26H; -CONHCH$_2$(CH_2)$_{13}$CH$_3$), 0.88 ppm (t, J = 6.2 Hz, 3H; -CONHCH$_2$(CH$_2$)$_{13}$CH_3; ^{13}C NMR (62.8 MHz, $CDCl_3$): 209.6 (-*C*=S), 165.9 (-*C*ONH-), 128.8 (-C=C-), 39.9 (-NH*C*H$_2$CH$_2$-), 39.3 (-S*C*H$_2$CONH-), 31.6, 29.3, 29.2, 29.1, 29.0, 26.7, 22.4 (-NHCH$_2$-(*C*H$_2$)$_{13}$CH$_3$), 19.0 (-S-*C*H$_3$), 13.8 ppm (-NH(CH$_2$)$_{14}$*C*H$_3$); elemental analysis calcd (%) for $C_{21}H_{37}NOS_5$: C 52.56, H 7.77, N 2.92; found: C 52.65, H 7.84, N 3.02.

4-(Thioacetooctadecylamido)-5-methylthio-1,3-dithiol-2-thione (8c): The procedure was the same as that described for **8a**, with **6** (2.10 g, 7.91 mmol), $CsOH·H_2O$ (1.33 g, 7.92 mmol) and **7c** (4.62 g, 13.3 mmol). In this case the column chromatography was done using $CHCl_3$ as eluent to give 2.77 g (67 %) of a yellow powder characterized as **8c**. M.p. 98.7 °C; FT-IR: $\tilde{\nu}$ = 3292 (m, NH), 2918 (s), 2849 (s), 1637 (s, CONH), 1544 (m, CONH), 1463 (m), 1418 (w), 1401 (w), 1315 (w), 1211 (w, C–N), 1160 (w), 1057 (m, C=S), 1031 (w), 945 (w), 898 (w), 721 cm^{-1} (w, NH); ^{1}H NMR (250 MHz, $CDCl_3$): δ = 6.52 (s, 1H; -SCH$_2$CON*H*-), 3.56 (s, 2H; -SCH_2CO-), 3.32 (q, J = 6.9 Hz, 2H; -CONHCH_2(CH$_2$)$_{16}$CH$_3$), 2.57 (s, 3H; -SCH_3), 1.28 (m, 32H; -CONHCH$_2$(CH_2)$_{16}$CH$_3$), 0.91 ppm (t, J = 6.2 Hz, 3H; -CONHCH$_2$(CH$_2$)$_{16}$CH_3; ^{13}C NMR (62.8 MHz,$CDCl_3$): δ = 209.5 (-*C*=S), 165.8 (-*C*ONH-), 128.7 (-C=C-), 39.9 (-NH*C*H$_2$CH$_2$-), 39.3 (-S*C*H$_2$CONH-), 31.6, 29.4, 29.3, 29.2, 29.2, 29.1, 29.0, 26.7, 22.4 (-NHCH$_2$(*C*H$_2$)$_{16}$CH$_3$), 19.0 (-S-*C*H$_3$), 13.8 ppm (-NH(CH$_2$)$_{17}$*C*H$_3$); elemental analysis calcd (%) for $C_{24}H_{43}NOS_5$: C 55.23, H 8.30, N 2.68; found: C 55.33, H 8.52, N 2.87.

4-(Thioacetododecylamido)-5-methylthio-1,3-dithiol-2-one (9a): Compound **8a** (2.28 g, 5.21 mmol) was dissolved with $Hg(OAc)_2$ (7.47 g, 23.4 mmol) in $CHCl_3$/HOAc (3:1, 180 mL) and was stirred at room temperature overnight under argon atmosphere. A Celite filter was required to remove the excess of $Hg(OAc)_2$. The solution was extracted with a saturated solution of $NaHCO_3$ (3×30 mL) and water (4×25 mL) The organic layer was dried ($MgSO_4$) and stripped of solvent and the oily residue was purified by flash column chromatography on silica gel ($CHCl_3$/EtOAc 95:5) to give 1.83 g (83 %) of **9a** as a white powder. M.p. 76.0 °C; FT-IR: $\tilde{\nu}$ = 3291 (m, NH), 2954 (s), 2921 (s), 2848 (s), 1672 (s, CONH),

1629 (s, CONH), 1547 (m, CONH), 1466 (w), 1425 (w), 1376 (w), 1265 (w, C–N), 1203 (w), 902 (w), 885 (w), 722 cm^{-1} (w, NH); ^1H NMR (250 MHz, $CDCl_3$): $\delta = 6.63$ (s, 1H; -SCH_2CONH-), 3.53 (s, 2H; -SCH_2CONH-), 3.29 (q, $J = 6.2$ Hz, 2H; -CONH $CH_2(CH_2)_{10}CH_3$), 2.51 (s, 3H; -SCH_3), 1.26 (m, 20H; -CONH $CH_2(CH_2)_{10}CH_3$), 0.88 ppm (t, $J =$ 6.2 Hz, 3H; -CONH $CH_2(CH_2)_{10}CH_3$); ^{13}C NMR (62.8 MHz,$CDCl_3$): $\delta =$ 188.4 (-C=O), 166.0 (-CONH-), 120.8 (-C=C-), 39.9 (-$NHCH_2CH_2$-), 39.3 (-SCH_2CONH-), 31.6, 29.3, 29.3, 29.2, 29.1, 29.0, 29.0, 26.7, 22.4 (-$NHCH_2(CH_2)_{10}CH_3$), 19.1 (-S-CH_3), 13.8 ppm (-$NH(CH_2)_{11}CH_3$); elemental analysis calcd (%) for $C_{18}H_{31}NO_2S_4$: C 51.27, H 7.41, N 3.32; found: C 51.37, H 7.50, N 3.35.

4-(Thioacetopentadecylamido)-5-methylthio-1,3-dithiol-2-one (9b): The method of synthesis and purification was that described for **9a**, but with **8b** (1.00 g, 2.08 mmol) and $Hg(OAc)_2$ (1.66 g, 5.21 mmol), and giving 0.84 g (87%) of a white solid. M.p. 75.8°C; FT-IR: $\tilde{\nu} = 3292$ (m, NH), 2956 (m), 2922 (s), 2848 (s), 1671 (s, CONH), 1627 (s, C=O), 1547 (m, CONH), 1464 (w), 1425 (w), 1314 (w), 1265 (w, C–N), 1201 (w), 903 (w), 886 (m), 723 cm^{-1} (w, NH); ^1H NMR (250 MHz, $CDCl_3$): $\delta = 6.62$ (s, 1H; -SCH_2CONH-), 3.53 (s, 2H; -SCH_2CONH-), 3,29 (q, $J = 6.7$ Hz, 2H; -CONH $CH_2(CH_2)_{13}CH_3$), 2.51 (s, 3H; -SCH_3), 1.29 (m, 20H; -CONH $CH_2(CH_2)_{13}CH_3$), 0.88 ppm (t, $J = 6.4$ Hz, 3H; -CONH $CH_2(CH_2)_{13}CH_3$); ^{13}C NMR (62.8 MHz,$CDCl_3$): $\delta = 188.6$ (-C=O), 165.9 (-CONH-), 120.7 (-C=C-), 39.9 (-$NHCH_2CH_2$-), 39.3 (-SCH_2CONH-), 31.6, 29.3, 29.3, 29.2, 29.1, 29.1, 29.0, 28.9, 26.7, 26.5, 22.4 (-$NHCH_2(CH_2)_{13}CH_3$), 19.2 (-S-CH_3), 13.8 ppm (-$NH(CH_2)_{14}CH_3$); elemental analysis calcd (%) for $C_{21}H_{37}NO_2S_4$: C 54.38, H 8.04, N 3.02; found: C 54.45, H 8.04, N 3.12.

4-(Thioacetooctadecylamido)-5-methylthio-1,3-dithiol-2-one (9c): The procedure was that used for **9a**, but with **8c** (4.00 g, 1.91 mmol) and $Hg(OAc)_2$ (6.11 g, 19.2 mmol). After workup, the oily residue was purified by flash column chromatography (SiO_2, $CHCl_3$:EtOAc (90:10)), giving 2.73 g (72%) of a white powder. M.p. 88.0°C; FT-IR: $\tilde{\nu} = 3292$ (m, NH), 2919 (s), 2850 (s), 1680 (s, CONH), 1643 (s, C=O), 1555 (m, CONH), 1467 (w), 1424 (w), 1324 (w), 1217 (w, C–N), 1154 (w), 901 (m), 720 cm^{-1} (w, NH); ^1H NMR (250 MHz, $CDCl_3$): $\delta = 6{,}63$ (s, 1H; -SCH_2CONH-), 3.53 (s, 2H; -SCH_2CONH-), 3.28 (q, $J = 6.7$ Hz, 2H; -CONH $CH_2(CH_2)_{16}CH_3$), 2.51 (s, 3H; -SCH_3), 1.26 (m, 32H; -CONH $CH_2(CH_2)_{16}CH_3$), 0.88 ppm (t, $J = 6.2$ Hz, 3H; -CONH $CH_2(CH_2)_{16}CH_3$); ^{13}C NMR (62.8 MHz,$CDCl_3$): $\delta = 188.3$ (-C=O), 165.9 (-CONH-), 120.7 (-C=C-), 39.9 (-$NHCH_2CH_2$-), 39.3 (-SCH_2CONH-), 31.6, 29.4, 29.3, 29.3, 29.1, 29.1, 29.0, 26.7, 22.4 (-$NHCH_2(CH_2)_{16}CH_3$), 19.2 (-S-CH_3), 13.8 ppm (-$NH(CH_2)_{17}CH_3$); elemental analysis calcd (%) for $C_{24}H_{43}NO_2S_4$: C 56.98, H 8.57, N 2.77; found: C 56.12, H 8.39, N 2.55.

2,7-Bis(methylthio)-3,6-bis(thioacetododecylamidotetrathiafulvalene) (2a) and 2,6-bis(thioacetododecylamido)-3,7-bis(methylthiotetrathiafulvalene) (1a): Compound **9a** (1.83 g, 4.34 mmol) was refluxed and stirred in dry trimethylphosphite (6 mL) under inert atmosphere for 7 h. The solution was cooled down and the trimethylphosphite was evaporated leaving an orange powder, which was purified by flash column chromatography (SiO_2, CH_2Cl_2/EtOAc 90:10) to collect **2a** and by increasing the proportion of EtOAc the *cis* isomer, **1a**, was collected. The amount of **2a** obtained was 277 mg (8%), and for **1a** is 269 mg (8%).

*Data for **1a***: M.p. 83°C; LDI-TOF/MS: *m/z* (%): 811 (100) $[M]^+$; FT-IR: $\tilde{\nu} = 3300$ (s, NH), 2915 (s), 2849 (s), 1646 (s, CONH), 1550 (m, CONH), 1470 (w), 1407 (w), 1377 (w), 1305 (w), 1218 (w, C–N), 1146 (w), 965 (w), 770 (w), 718 cm^{-1} (w, NH); ^1H NMR (250 MHz, $CDCl_3$): $\delta = 6.75$ (s, 2H; -SCH_2CONH-), 3.50 (s, 4H; -SCH_2CONH-), 3.28 (q, $J = 6.2$ Hz, 4H; -CONH $CH_2(CH_2)_{10}CH_3$), 2.46 (s, 6H; -SCH_3), 1.26 (m, 40H; -CONH $CH_2(CH_2)_{10}CH_3$), 0.88 ppm (t, $J = 6.2$ Hz, 6H; -CONH $CH_2(CH_2)_{10}CH_3$).

*Data for **2a***: M.p. 98°C; LDI-TOF/MS: *m/z* (%): 811 (100) $[M]^+$; FT-IR: $\tilde{\nu} = 3299$ (s, NH), 2915 (s), 2850 (m), 1645 (s, CONH), 1551 (s, CONH), 1470 (w), 1408 (w), 1146 (m), 1098 (m), 885 (w), 770 (w), 718 cm^{-1} (w, NH); ^1H NMR (250 MHz, $CDCl_3$): $\delta = 6.84$ (s, 2H; -SCH_2CONH-), 3.51 (s, 4H; -SCH_2CONH-), 3.28 (q, $J = 6.9$ Hz, 4H; -CONH $CH_2(CH_2)_{10}CH_3$), 2.47 (s, 6H; -SCH_3), 1.26 (m, 40H; -CONH $CH_2(CH_2)_{10}CH_3$), 0.88 ppm (t, $J = 6.4$ Hz, 6H; -CONH $CH_2(CH_2)_{10}CH_3$); elemental analysis calcd (%) for $C_{36}H_{62}N_2O_2S_8$: C 53.29, H 7.70, N 3.45; found: C 53.15, H 7.80, N 3.55.

2,7-Bis(methylthio)-3,6-bis(thioacetopentadecylamidotetrathiafulvalene) (2b) and 2,6-bis(thioacetopentadecylamido)-3,7-bis(methylthiotetrathiafulvalene) (1b): The procedure for the synthesis of the two compounds was that described for **2a** and **1a**. The coupling was done with **9b** (0.72 g, 1,54 mmol) and to purify the orange solid the same eluent (CH_2Cl_2/EtOAc (90:10)) and the same method were used to give 179 mg (13%) of **1b** and 124 mg (9%) of **2b**.

*Data for **1b***: M.p. 87°C; LDI-TOF/MS: *m/z* (%): 895 (100) $[M]^+$; FT-IR: $\tilde{\nu} = 3298$ (s, NH), 2955 (m), 2915 (s), 2849 (s), 1644 (s, CONH), 1554 (s, CONH), 1470 (w), 1408 (w), 1317 (w), 1301 (w), 1221 (w, C–N), 1149 (w), 1080 (w), 886 (w), 718 cm^{-1} (w, NH); ^1H NMR (250 MHz, $CDCl_3$): $\delta = 6.84$ (s, 2H; -SCH_2CONH-), 3.51 (s, 4H; -SCH_2CONH-), 3.28 (q, $J =$ 6.7 Hz, 4H; -CONH $CH_2(CH_2)_{13}CH_3$), 2.47 (s, 6H; -SCH_3), 1.26 (m, 52H; -CONH $CH_2(CH_2)_{13}CH_3$), 0.88 ppm (t, $J = 6.2$ Hz, 6H; -CONH $CH_2(CH_2)_{13}CH_3$); elemental analysis calcd (%) for $C_{42}H_{74}N_2O_2S_8$: C 56.33, H 8.33, N 3.13; found: C 56.42, H 8.25, N 3.12.

*Data for **2b***: M.p. 92°C; LDI-TOF/MS: *m/z* (%): 895 (100) $[M]^+$; FT-IR: $\tilde{\nu} = 3298$ (m, NH), 2955 (w), 2920 (s), 2851 (s), 1644 (s, CONH), 1554 (m, CONH), 1468 (w), 1406 (w), 1317 (w), 1219 (w, C–N), 1149 (w), 720 cm^{-1} (w, NH); ^1H NMR (250 MHz, $CDCl_3$): $\delta = 6.79$ (s, 2H; -SCH_2CONH-), 3.50 (s, 4H; -SCH_2CONH-), 3.26 (q, $J = 6.7$ Hz, 4H; -CONH $CH_2(CH_2)_{13}CH_3$), 2.45 (s, 6H; -SCH_3), 1.25 (m, 52H; -CONH $CH_2(CH_2)_{13}CH_3$), 0.88 ppm (t, $J = 6.2$ Hz, 6H; -CONH $CH_2(CH_2)_{13}CH_3$); elemental analysis calcd (%) for $C_{42}H_{74}N_2O_2S_8$: C 56.33, H 8.33, N 3.13; found: C 56.26, H 8.20, N 3.17.

2,7-Bis(methylthio)-3,6-bis(thioacetooctadecylamidetetrathiafulvalene) (2c) and 2,6-bis(thioacetooctadecylamide)-3,7-bis(methylthiotetrathiafulvalene) (1c): The method used was that reported above for **1a** and **2a**. The starting compound **9c** (2.08 g, 4.11 mmol) was dissolved in trimethylphosphite (6 mL). The purifications was done as for the other TTF derivatives to give 317 mg (8%) of **1c** and 156 mg (4%) of **2c**.

*Data for **1c***: M.p. 106°C; LDI-TOF/MS: *m/z* (%): 978 (100) $[M]^+$; FT-IR: $\tilde{\nu} = 3300$ (m, NH), 2916 (s), 2849 (s), 1644 (s, CONH), 1551 (m, CONH), 1471 (w), 1146 (w), 885 (w), 717 cm^{-1} (w, NH); ^1H NMR (250 MHz, $CDCl_3$): $\delta = 6.87$ (s, 2H; -SCH_2CONH-), 3.53 (s, 4H; -SCH_2CONH-), 3.31 (q, $J = 6.9$ Hz, 4H; -CONH $CH_2(CH_2)_{16}CH_3$), 2.49 (s, 6H; -SCH_3), 1.28 (m, 64H; -CONH $CH_2(CH_2)_{16}CH_3$), 0.91 ppm (t, $J =$ 6.2 Hz, 6H; -CONH $CH_2(CH_2)_{16}CH_3$); elemental analysis calcd (%) for $C_{48}H_{86}N_2O_2S_8$: C 58.84, H 8.85, N 2.86; found: C 58.96, H 8.76, N 3.00.

*Data for **2c***: M.p. 119°C; LDI-TOF/MS: *m/z* (%): 978 (100) $[M]^+$; FT-IR: $\tilde{\nu} = 3300$ (m, NH), 2916 (s), 2850 (s), 1645 (s, CONH), 1554 (m, CONH), 1470 (w), 1409 (w), 1314 (w), 1217 (w, C–N), 1146 (w), 1028 (w), 718 cm^{-1} (w, NH); ^1H NMR (250 MHz, $CDCl_3$): $\delta = 6.80$ (s, 2H; -SCH_2CONH-), 3.53 (s, 4H; -SCH_2CONH-), 3.29 (q, $J = 7.2$ Hz, 4H; -CONH $CH_2(CH_2)_{16}CH_3$), 2.48 (s, 6H; -SCH_3), 1.28 (m, 64H; -CONH $CH_2(CH_2)_{16}CH_3$), 0.91 ppm (t, $J = 6.3$ Hz, 6H; -CONH $CH_2(CH_2)_{16}CH_3$).

2,7-Bis(acetoxydodecylamido)naphthalene (3): Naphthalene-2,7-diol (1.00 g, 6,24 mmol, from Aldrich) and **7a** (3.92 g, 14.97 mmol) were dissolved in CH_3CN (80 mL) and potassium carbonate (5.17 g, 37.41 mmol) was added. The mixture was refluxed overnight under an inert atmosphere. The cooled solution was filtered and the solid residue was washed with MeCN, then dissolved in CH_2Cl_2/EtOAc (1:1) and filtered, and the solvent evaporated leaving a white powder characterized as compound **3** (2.32 g, 61%). M.p. 147°C; LDI-TOF/MS: *m/z* (%): 611 (100) $[M]^+$; FT-IR: $\tilde{\nu} = 3388$ (m, NH), 2917 (f), 2849 (s), 1658 (s, CONH), 1549 (m, CONH), 1468 (w), 1392 (w), 1216 (w), 1168 (w), 1052 (w), 843 (w), 720 (w), 583 cm^{-1} (w, NH); ^1H NMR (250 MHz, $CDCl_3$): $\delta = 7.73$, 7.69 (d, $J =$ 9.8 Hz, 2H; -HC=CH-), 7.09 (s, 2H; -HC=), 7.08, 7.05 (d, $J = 8{,}5$ Hz, 2H; -HC=CH-), 6,62 (s, 2H; -OCH_2CONH-), 4.58 (s, 4H; -OCH_2CONH-), 3.35 (q, $J = 6.7$ Hz, 4H; -CONH $CH_2(CH_2)_{10}CH_3$), 1.23 (m, 40H; -CONH $CH_2(CH_2)_{10}CH_3$), 0.87 ppm (t, $J = 6.3$ Hz, 6H; -CONH $CH_2(CH_2)_{10}CH_3$); ^{13}C NMR (62.8 MHz,$CDCl_3$): $\delta = 167.5$ (-CONH-), 155.6 (O-C aromatic), 135.2 (C=C aromatic central), 129.4 (C=C aromatic), 125.1 (C=C aromatic central), 115.9 (C=C aromatic), 106.9 (C=C aromatic), 67.1 (-OCH_2CONH-), 38.8 (-$NHCH_2CH_2$-), 31.6, 29.3, 29.3, 29.2, 29.0, 28.9, 26.6, 22.4, (-$NHCH_2(CH_2)_{10}CH_3$), 13.8 ppm (-$NH(CH_2)_{11}CH_3$); elemental analysis calcd (%) for $C_{38}H_{62}N_2O_4$: C 74.71, H 10.23, N 4.59; found: C 74.60, H 10.16, N 4.57.

2,6-Bis(acetoxydodecylamido)naphthalene (4): Commercial naphthalene-2,6-diol (1.00 g, 6.24 mmol) and **7a** (3.92 g, 14.97 mmol) were dissolved toluene/THF (1:1, 80 mL) and potassium carbonate (3.88 g, 28.09 mmol) was added. The resulting solution was refluxed overnight. The desired compound was purified as described for **3**, giving 1.58 g (42 %) of an off-white solid. M.p. 160 °C; LDI-TOF/MS: m/z (%): 611 (100) $[M]^+$; FT-IR: $\tilde{\nu}$ = 3366 (m, NH), 2919 (s), 2849 (s), 1654 (s, CONH), 1536 (m, CONH), 1470 (w), 1394 (w), 1231 (w), 1164 (w), 1064 (w), 848 (w), 722 (w), 584 cm^{-1} (w, NH); ^{1}H NMR (250 MHz, $CDCl_3$): δ = 7.71, 7.68 (d, J = 8.9 Hz, 2H; -HC=CH-), 7.26 (s, 1H; -HC=), 7.21, 7.18 (d, J = 8.9 Hz, 2H; -HC=CH-), 7.11 (s, 1H; -HC=), 6.61 (s, 2H; -OCH_2CONH-), 4.59 (s, 4H; -OCH_2CONH-), 3.35 (q, J = 6.7 Hz, 4H; -CONH $CH_2(CH_2)_{10}CH_3$), 1.24 (m, 40H; -CONH $CH_2(CH_2)_{10}CH_3$), 0.88 ppm (t, J = 6.3 Hz, 6H; -CONH $CH_2(CH_2)_{10}CH_3$); ^{13}C NMR (62.8 MHz,$CDCl_3$): δ = 167.7 (-CONH-), 153.8 (O-Caromatic), 129.8 (C=C aromatic), 128.6 (C=C aromatic), 118.6 (C=C aromatic), 107.5 (C=C aromatic), 67.2 (-OCH_2CONH-), 38.8 (-$NHCH_2CH_2$-), 31.6, 29.3, 29.3, 29.2, 29.1, 29.0, 26.6, 22.4, (-$NHCH_2$-$(CH_2)_{10}CH_3$), 13.8 ppm (-$NH(CH_2)_{11}CH_3$); elemental analysis calcd (%) for $C_{38}H_{62}N_2O_4$: C 74.71, H 10.23, N 4.59; found: C 74.64, H 10.17, N 4.61.

4,4′-Bis(acetoxydodecylamido)bisphenyl (5): 4,4′-Dihydroxybiphenyl (0.9 g, 4.83 mmol), potassium carbonate (4.10 g, 29.66 mmol) and **7a** (3.04 g, 11.60 mmol) were reacted together by using the same procedure described for **3**. The yield of the reaction was 81 % (2.50 g) of a white solid characterized as compound **5**. M.p. 182 °C; LDI-TOF/MS: m/z (%): 637 (100) $[M]^+$; FT-IR: $\tilde{\nu}$ = 3299 (m, NH), 2918 (s),2849 (s), 1653 (s, CONH), 1544 (m, CONH), 1501 (w), 1469 (w), 1286 (w), 1180 (w), 1063 (w), 821(w), 720 (w), 590 cm^{-1} (w, NH); ^{1}H NMR (250 MHz, $CDCl_3$): δ = 7.51, 7.47 (d, J = 8.8 Hz, 4H; -HC=CH-), 7.00, 6.96 (d, J = 8.8 Hz, 4H; -HC=CH-), 6.60 (s, 2H; -OCH_2CONH-), 4.51 (s, 4H; -OCH_2CONH-), 3.34 (q, J = 6,7 Hz, 4H; -CONH $CH_2(CH_2)_{10}CH_3$), 1.24 (m, 40H; -CONH $CH_2(CH_2)_{10}CH_3$), 0.87 ppm (t, J = 6.3 Hz, 6H; -CONH $CH_2(CH_2)_{10}CH_3$); ^{13}C NMR (62.8 MHz,$CDCl_3$): δ = 167.7 (-CONH-), 156.3 (O-Caromatic), 134,2 (C=C aromatic), 127.9 (C=C aromatic), 114.7 (C=C aromatic), 67.3 (-OCH_2CONH-), 38.8 (-$NHCH_2CH_2$-), 31.6, 29.3, 29.3, 29.2, 29.1, 29.0, 26.6, 22.4, (-$NHCH_2(CH_2)_{10}CH_3$), 13.8 ppm (-$NH(CH_2)_{11}CH_3$); elemental analysis calcd (%) for $C_{40}H_{64}N_2O_4$: C 75.43, H 10.13, N 4.40; found: C 75.58, H 10.04, N 4.47.

Acknowledgements

This work was supported by the DGI, Spain (Project No. BQU 2003-00760), the Belgian Federal Science Policy Office (PAI 5/3), FNRS, and the Marie Curie Research Training Network CHEXTAN (MRTN-CT-2004-512161). J.P. thanks the Generalitat de Catalunya for a pre-doctoral grant, linked with the Fundació Institut Català de Nanotecnologia. A.L. and G.U. acknowledge the Generalitat de Catalunya, (project 2005/SGR/00896) and the Spanish MEC for Grant no. CTQ2005-09000-C02-01, and a "Ramon y Cajal" contract to G.U. We warmly thank Amable Bernabé for recording IR and LDI-TOF spectra. We thank Hiroshi Uji-i and Steven De Feyter for fruitful discussions.

[1] R. L. Carroll, C. B. Gorman, *Angew. Chem.* **2002**, *114*, 4556–4579; *Angew. Chem. Int. Ed.* **2002**, *41*, 4378–4400.
[2] G. Maruccio, R. Cingolani, R. Rinaldi, *J. Mater. Chem.* **2004**, *14*, 542–554.
[3] K. Nørgaard, T. Bjørnholm, *Chem. Commun.* **2005**, 1812.
[4] "Molecular Electronics III": *Ann. N.Y. Acad. Sci.* **2003**, *1006*, whole volume.
[5] C. M. Lieber, *MRS Bull.* **2003**, *28*, 486–491.
[6] A. H. Flood, R. J. A. Ramirez, W. Q. Deng, R. P. Muller, W. A. Goddard, J. F. Stoddart, *Aust. J. Chem.* **2004**, *57*, 301–322.
[7] M. Cavallini, M. Facchini, M. Massi, F. Biscarini, *Synth. Met.* **2004**, *146*, 283–286.
[8] A. P. H. J. Schenning, E. W. Meijer, *Chem. Commun.* **2005**, 3245–3258.
[9] "Supramolecular Engineering of Synthetic Metallic Materials"*NATO ASI Ser. Ser. C* **1999**, *518*, whole volume.
[10] Q. Guo, J. Yin, F. Yin, R. E. Palmer, N. Bampos, J. K. M. Sanders, *J. Phys.-Cond. Matter.* **2003**, *15*, S3127-S3138.
[11] V. Palermo, M. Palma, Z. Tomovic, M. D. Watson, K. Müllen, P. Samorì, *Synth. Metals* **2004**, *147*, 117–121.
[12] G. Ridolfi, L. Favaretto, G. Barbarella, P. Samorì, N. Camaioni, *J. Mater. Chem.* **2005**, *15*, 1704–1707.
[13] M. Kastler, W. Pisula, D. Wasserfallen, T. Pakula, K. Mullen, *J. Am. Chem. Soc.* **2005**, *127*, 4286–4296.
[14] A. Arena, S. Patane, G. Saitta, A. Bonavita, *Mater. Lett.* **2006**, *60*, 2171–2174.
[15] E. Rabani, D. R. Reichman, P. L. Geissler, L. E. Brus, *Nature* **2003**, *426*, 271–274.
[16] H. Yao, T. Isohashi, K. Kimura, *Chem. Phys. Lett.* **2004**, *396*, 316–322.
[17] X. J. Zhang, X. H. Zhang, W. S. Shi, X. M. Meng, C. Lee, S. Lee, *J. Phys. Chem. B* **2005**, *109*, 18777–18780.
[18] N. Liu, X. Wang, H. Cao, C. H. Chen, W. J. Zhang, Y. Wei, *Macromol. Rapid Commun.* **2005**, *26*, 1925–1930.
[19] M. Ferrari, F. Ravera, M. Viviani, L. Liggieri, *Colloids Surf. A* **2004**, *249*, 63–67.
[20] M. T. Stone, J. M. Heemstra, J. S. Moore, *Acc. Chem. Res.* **2006**, *39*, 11–20.
[21] E. Aret, V. Volotchaev, S. Verhaegen, H. Meekes, E. Vlieg, G. Deroover, C. van Roost, *Cryst. Growth Des.* **2006**, *6*, 1027–1032.
[22] M. Rittner, P. Baeuerle, G. Goetz, H. Schweizer, F. J. B. Calleja, M. H. Pilkuhn, *Synth. Met.* **2006**, *156*, 21–26.
[23] M. M. S. Abdel-Mottaleb, E. Gomar-Nadal, M. Surin, H. Uji-I, W. Mamdouh, J. Veciana, V. Lemaur, C. Rovira, J. Cornil, R. Lazzaroni, D. B. Amabilino, S. De Feyter, F. C. De Schryver, *J. Mater. Chem.* **2005**, *15*, 4601–4615.
[24] D. J. Liu, S. De Feyter, M. Cotlet, U. M. Wiesler, T. Weil, A. Herrmann, K. Müllen, F. C. De Schryver, *Macromolecules* **2003**, *36*, 8489–8498.
[25] C. C. Dupont-Gillain, I. Jacquemart, P. G. Rouxhet, *Colloids Surf. B* **2005**, *43*, 179–186.
[26] V. Palermo, S. Morelli, C. Simpson, K. Müllen, P. Samorì, *J. Mater. Chem.* **2006**, *16*, 266–271.
[27] J. Malthête, A.-M. Levelut, L. Liébert, *Adv. Mater.* **1992**, *4*, 37–41.
[28] E. A. Archer, H. Gong, M. J. Krische, *Tetrahedron* **2001**, *57*, 1139–1159.
[29] J. J. van Gorp, J. A. J. M. Vekemans, E. W. Meijer, *J. Am. Chem. Soc.* **2002**, *124*, 14759–14769.
[30] M. Shirakawa, S.-i. Kawano, N. Fujita, K. Sada, S. Shinkai, *J. Org. Chem.* **2003**, *68*, 5037–5044.
[31] F. M. Menger, H. Zhang, *Langmuir* **2005**, *21*, 10428–10438.
[32] H. C. Li, J. O. Jeppesen, E. Levillain, J. Becher, *Chem. Commun.* **2003**, 846–847.
[33] X. W. Xiao, W. Xu, D. Q. Zhang, H. Xu, H. Y. Lu, D. B. Zhu, *J. Mater. Chem.* **2005**, *15*, 2557–2561.
[34] E. Gomar-Nadal, J. Veciana, C. Rovira, D. B. Amabilino, *Adv. Mater.* **2005**, *17*, 2095–2098.
[35] Y. Liu, S. Saha, S. A. Vignon, A. H. Flood, J. F. Stoddart, *Synthesis* **2005**, 3437–3445.
[36] P. T. Chiang, P. N. Cheng, C. F. Lin, Y. H. Liu, C. C. Lai, S. M. Peng, S. H. Chiu, *Chem. Eur. J.* **2006**, *12*, 865–876.
[37] M. R. Bryce, *Chem. Soc. Rev.* **1991**, *20*, 355–390.
[38] *Handbook of organic conductive molecules and polymers, Vol. 1* (Ed.: N. S. Nalwa), Wiley, New York, **1997**.
[39] M. Mas-Torrent, C. Rovira, *J. Mater. Chem.* **2006**, *16*, 433–436.
[40] X. Gao, W. Wu, Y. Liu, W. Qiu, X. Sun, G. Yu, D. Zhu, *Chem. Commun.* **2006**, 2750–2752.
[41] A. S. Batsanov, M. R. Bryce, G. Cooke, A. S. Dhindsa, J. N. Heaton, J. A. K. Howard, A. J. Moore, M. C. Petty, *Chem. Mater.* **1994**, *6*, 1419–1425.

[42] O. Neilands, S. Belyakov, V. Tilika, A. Edzina, *J. Chem. Soc. Chem. Commun.* **1995**, 325–326.
[43] A. J. Moore, M. R. Bryce, A. S. Batsanov, J. N. Heaton, C. W. Jehmann, J. A. K. Howard, N. Robertson, A. E. Underhill, I. F. Perepichka, *J. Mater. Chem.* **1998**, *8*, 1541–1550.
[44] K. Heuzé, M. Fourmigué, P. Batail, *J. Mater. Chem.* **1999**, *9*, 2373–2379.
[45] K. Heuzé, M. Fourmigué, P. Batail, E. Canadell, P. Auban-Senzier, *Chem. Eur. J.* **1999**, *5*, 2971–2976.
[46] J.-P. Griffiths, A. A. Arola, G. Appleby, J. D. Wallis, *Tetrahedron Lett.* **2004**, *45*, 2813–2816.
[47] R. J. Brown, G. Camarasa, J.-P. Griffiths, P. Day, J. D. Wallis, *Tetrahedron Lett.* **2004**, *45*, 5103–5107.
[48] G. Ono, A. Izuoka, T. Sugawara, Y. Sugawara, *J. Mater. Chem.* **1998**, *8*, 1703–1709.
[49] M. Jørgensen, K. Bechgaard, T. Bjørnholm, O. Sommer-Larsen, L. G. Hansen, K. Schaumburg, *J. Org. Chem.* **1994**, *59*, 5877–5882.
[50] D. R. Talham, *Chem. Rev.* **2004**, *104*, 5479–5501.
[51] J. Sly, P. Kasák, E. Gomar-Nadal, C. Rovira, L. Górriz, P. Thordarson, D. B. Amabilino, A. E. Rowan, R. J. M. Nolte, *Chem. Commun.* **2005**, 1255–1257.
[52] T. Kitahara, M. Shirakawa, S.-i. Kawano, U. Beginn, N. Fujita, S. Shinkai, *J. Am. Chem. Soc.* **2005**, *127*, 14980–14981.
[53] T. Kitamura, S. Nakaso, N. Mizoshita, Y. Tochigi, T. Shimomura, M. Moriyama, K. Ito, T. Kato, *J. Am. Chem. Soc.* **2005**, *127*, 14769–14775.
[54] J. Puigmartí-Luis, V. Laukhin, Á. Pérez del Pino, J. Vidal-Gancedo, C. Rovira, E. Laukhina, D. B. Amabilino, *Angew. Chem.* DOI: 10.1002/ange.200602483; *Angew. Chem. Int. Ed.* 10.1002/anie.200602483.
[55] E. Gomar-Nadal, M. M. S. Abdel-Mottaleb, S. De Feyter, J. Veciana, C. Rovira, D. B. Amabilino, F. C. De Schryver, *Chem. Commun.* **2003**, 906–907.
[56] C. A. Hunter, K. R. Lawson, J. Perkins, C. J. Urch, *J. Chem. Soc. Perkin Trans. 2* **2001**, 651–669.
[57] G. Lincke, *Dyes Pigm.* **2003**, *59*, 1–24.
[58] I. Huc, *Eur. J. Org. Chem.* **2004**, 17–29.
[59] R. Vilar, *Struct. Bonding* **2004**, *111*, 85–137.
[60] H. Inokuchi, G. Saito, P. Wu, K. Seki, T. B. Tang, T. Mori, K. Imaeda, T. Enoki, Y. Higuchi, K. Inaka, N. Yasuoka, *Chem. Lett.* **1986**, 1263–1266.
[61] K. B. Simonsen, N. Svenstrup, J. Lau, O. Simonsen, P. Mørk, G. J. Kristensen, J. Becher, *Synthesis* **1996**, 407–418.
[62] T. Thorsteinsson, M. Másson, K. G. Kristinsson, M. A. Hjálmarsdóttir, H. Hilmarsson, T. Loftsson, *J. Med. Chem.* **2003**, *46*, 4173–4181.
[63] Y. Kubo, Y. Kitada, R. Wakabayashi, T. Kishida, M. Ayabe, K. Knaeko, M. Takeuchi, S. Shinkai, *Angew. Chem.* **2006**, *118*, 1578–1583.; *Angew. Chem.* **2006**, *118*, 1578–1583; *Angew. Chem. Int. Ed.* **2006**, *45*, 1548–1553.
[64] T.-Q. Nguyen, M. L. Bushey, L. E. Brus, C. Nuckolls, *J. Am. Chem. Soc.* **2002**, *124*, 15051–15054.
[65] K. E. Strawhecker, S. K. Kumar, J. F. Douglas, A. Karim, *Macromolecules* **2001**, *34*, 4669–4672.
[66] J. K. J. van Duren, X. N. Yang, J. Loos, C. W. T. Bulle-Lieuwma, A. B. Sieval, J. C. Hummelen R. A. J. Janssen, *Adv. Funct. Mater.* **2004**, *14*, 425–434.
[67] M. M. S. Abdel-Mottaleb, E. Gomar-Nadal, S. De Feyter, M. Zdanowska, J. Veciana, C. Rovira, D. B. Amabilino, F. C. De Schryver, *Nano. Lett.* **2003**, *3*, 1375–1378.
[68] M. Mas-Torrent, E. Laukhina, C. Rovira, J. Veciana, V. Tkacheva, L. Zorina, S. Khasanov, *Adv. Funct. Mater.* **2001**, *11*, 299–303.
[69] E. Laukhina, V. Tkacheva, S. Khasanov, L. Zorina, J. Gomez-Segura, A. Pérez del Pino, J. Veciana, V. Laukhin, C. Rovira, *ChemPhysChem* **2006**, *7*, 920–923.
[70] C. G. Wu, S. S. Chang, *J. Phys. Chem. B* **2005**, *109*, 825–832.
[71] A. Alexeev, J. Loos, M. M. Koetse, *Ultramicroscopy* **2006**, *106*, 191–199.
[72] J. W. Ponder, TINKER: Software Tools for Molecular Design, 4.2, Washington University School of Medicine, Saint Louis, MO, **2004**.

Received: July 27, 2006
Published online: November 22, 2006

